Applied Physics Research; Vol. 6, No. 6; 2014
ISSN 1916-9639 E-ISSN 1916-9647
Published by Canadian Center of Science and Education

Determination of Optical Properties of Undoped Amorphous Selenium (a-Se) Films by Dielectric Modeling of Their Normal-Incidence Transmittance Spectra

Mahmoud H. Saleh[1], Mousa M. Abdul-Gader Jafar[2], Basim N. Bulos[2] & Tariq M. F. Al-Daraghmeh[2]

[1] Department of Applied Sciences, Faculty of Engineering Technology, Al-Balqa′ Applied University, Amman 11134, Jordan

[2] Department of Physics, Faculty of Science, The University of Jordan, Amman 11942, Jordan

Correspondence: Mousa M. Abdul-Gader Jafar, Department of Physics, Faculty of Science, The University of Jordan, Amman 11942, Jordan. E-mail: mmjafar@ju.edu.jo

Received: September 19, 2014 Accepted: October 15, 2014 Online Published: October 21, 2014

doi:10.5539/apr.v6n6p10 URL: http://dx.doi.org/10.5539/apr.v6n6p10

Abstract

Normal-incidence specular transmittance $T_{\mathrm{exp}}(\lambda)$ of undoped amorphous selenium (a-Se) films of several thicknesses ($0.25-1\ \mu\mathrm{m}$) thermally evaporated on thick microscopic glass-slide substrates upheld at temperatures near 30 ℃ (below glass transition temperature of undoped Se) has been measured at room temperature in the spectral wavelength λ range $300-1100$ nm. Above a threshold wavelength λ_{c} (~ 600 nm), their as-measured $T_{\mathrm{exp}}(\lambda)-\lambda$ curves display transmittance values near that of glass substrates and exhibit well-resolved interference-fringe maxima and minima, signifying good uniformity of fabricated a-Se films. Below λ_{c}, the $T_{\mathrm{exp}}(\lambda)-\lambda$ curves decline progressively to zero transmittance, preceded by a tailing-like trend of possible structural disorder origin. The spectral dependencies of optical constants $n(\lambda)$ and $\kappa(\lambda)$ of the studied a-Se films on λ were retrieved from iterative curve-fitting of their $T_{\mathrm{exp}}(\lambda)$ – λ data to theoretical $T_{\mathrm{theor}}(\lambda)$-formulations of an *air-supported* {thin film/thick substrate}-stack using the O'Leary-Johnson-Lim (OJL) interband-transition dielectric model, combined with a dielectric constant ϵ_{∞}, representing the dielectric background at very high photon energies (at spectral wavelengths much smaller than measured). Regardless of the number of observed interference fringes, reliable simulation to the as-measured normal-incidence $T_{\mathrm{exp}}(\lambda)-\lambda$ spectra has been achieved, but were remarkably curve-fitted if we presume that a thin roughness layer (<5 nm) of selenium was formed on top of the fabricated undoped a-Se films. The retrieved $n(\lambda)-\lambda$ spectra display a broad peak around $\lambda\cong 0.52\ \mu\mathrm{m}$, below which $n(\lambda)$ was found to vary with wavelength in accordance with a Sellmeier-like (Wemple-DiDominco) single-oscillator (normal) dispersion formula, with a static index of refraction $n(E=0)=\sqrt{\epsilon_{\mathrm{s}}}\cong 2.42$, where ϵ_{s} is the static dielectric constant of the material at zero photon energy E, and an oscillator "average" bandgap energy of $E_{\mathrm{o}}\cong 3.93$ eV $\cong 2\,E_{\mathrm{g}}^{\mathrm{opt}}$, the optical (Tauc) bandgap energy. The values of $E_{\mathrm{g}}^{\mathrm{opt}}$ of studied undoped a-Se films deduced from Tauc-like plots were around 1.92 eV ($\pm$ 0.02 eV) and the retrieved values of OJL band-tailing energy parameter γ (Urbach-tail parameter Γ_{U}) was found to be in the range $40-50$ meV, slightly dependent on film thickness.

Keywords: a-Se films, transmittance, optical constants, OJL model, SCOUT software

1. Introduction

Amorphous selenium (a-Se) is endorsed to have a number of interesting technological applications, for instant, as a photoconductive thick layer in direct conversion flat-panel digital X-ray medical diagnostic imaging systems and in high-gain avalanche rushing photoconductor (HARP) video cameras that are based on avalanche multiplication (Kubota et al., 1996; Kasap & Rowlands, 2000; Kasap, 2002; Kasap et al., 2006; Zhao et al., 2005) and as a lateral (coplanar) metal-semiconductor-metal (MSM) photoconductor in indirect conversion X-ray imaging detection systems (Wang et al., *Appl. Phys. Lett*., 2009; Wang et al., *Proc. SPIE,* 2009; Wang et al., 2010). Thin selenium films also found a booming way in the fabrication of other solid-state devices such as Schottky diodes, solar cells and photovoltaic junctions (Ito et al., 1982; Touihri et al., 1997; Bernede et al., 1998; Lakshmi, 2001; Mukolu, 2004; Iyayi & Oberafo, 2005; Joshi & Lokhande, 2006; El-Nahass et al., 2006). Undoped a-Se is a typical p-type semiconducting chalcogenide glassy material with a high dc dark electrical resistivity ($10^{13}\ \Omega\,\mathrm{cm}$ at 300 K)

(Mott & Davis, 1979; Kolobov, 1996; Abdul-Gader et al., 1998; El-Zawawi & Abd-Alla, 1999); however, its glass-transformation temperature T_G is low (below 50 ℃, depending on its definition and experimental procedure used to define it (Grenet et al., 1980; Larmagnac et al., 1981; Kasap & Juhasz, 1986; Kasap et al., 1990; Pejova & Grozdanov, 2001; Tonchev & Kasap, 2002)). Thus, it is only possible to exploit inherent physical properties of as-deposited undoped *a*-Se films at low ambient temperatures, after ageing them in dark and humidity-free environment to reach structural relaxation. Extrinsic doping increases glass transformation and crystallization temperatures of *a*-Se films, often referred to as stabilized *a*-Se when slightly doped with arsenic (As), to limit deterioration of their performance with temperature and time when are incorporated in solid-state devices (Tan, 2006; Tan et al., 2007; Tan et al., 2006; Vautier et al., 1988; Bettstelleret al., 1993; Mulama et al., 2014; Benkhedir, 2006; Solieman et al., 2014). Reduction of time-ageing and glass transformation of undoped *a*-Se films, and hence virtuous performance in devices integrating them, can also be realized by growing and/or annealing them at temperatures around 70 ℃, but their electrical resistivity is significantly reduced (Abdul-Gader et al., 1998; Abdul-Gader & Nigmatullin, 2001; Al-Hamarneh et al., 2009). To fabricate undoped *a*-Se films, care should be taken not to grow them at temperatures higher than 45 ℃, not to expose it to intense nuclear radiations or illumination with photon energies close to its band-gap energy (El-Zawawi & Abd-Alla, 1999; Ishida & Tanaka, 1997; Poborchii et al., 1998; Innami & Adachi, 1999), and to store them under vacuum and dark conditions to impede deterioration and drastic change of their properties.

The design of optoelectronic devices that embrace thin/thick films made of semiconducting (insulating) materials, however, requires in part accurate determination of their optical constants and proper understanding of their optical and electronic behavior under various experimental conditions. The optical and electronic properties of ill-fabricated semiconducting films can significantly affect the performance of the device integrating them. Regarding optical properties of undoped *a*-Se films, a lot of work were carried out for decades, but this issue is still continue to receive research attention as the existing information on their optical behavior is still less than adequate and disperse. The reported literature values of room-temperature band-gap energy of undoped or slightly-doped *a*-Se scatter greatly in the range ($1.4 - 2.2$ eV) and the values of their optical constants vary from one work to another (Mott & Davis, 1979; Tan, 2006; Tan et al., 2007; Tan et al., 2006; Vautier et al., 1988; Bettstelleret al., 1993; Adachi & Kao1980; Kotkata & Abdel-Wahab, 1990; Kotkata et al., 2009; Navarrete et al., 1990; Solieman & Abu-Sehly, 2010; Nagels et al., 1995; Tichy et al., 1996; Nagels et al., 1997; Innami et al., 1999). The diversity of these findings may be related to different film thicknesses, to dissimilar methods and preparation conditions used in film deposition, and to variability of experimental techniques used to characterize optical response of studied films. Discrepancies in reported optical properties of undoped *a*-Se films may also be linked to techniques employing different theoretical formulations for analyzing measured optical data, and to the interband transition mechanisms and band-energy structure models used for interpreting the optical absorption phenomena operative in them (Mott & Davis, 1979; Tan et al., 2006; Vautier et al., 1988; Bettstelleret al., 1993; Mulama et al., 2014; Benkhedir, 2006; Adachi & Kao1980; Kotkata & Abdel-Wahab, 1990; Kotkata et al., 2009; Navarrete et al., 1990; Solieman & Abu-Sehly, 2010; Nagels et al., 1995; Tichy et al., 1996; Nagels et al., 1997; Innami et al., 1999).

To resolve part of the discrepancies noted in the reported literature findings on optical properties of *a*-Se and to enrich the literature with additional features and knowledge of dispersion and optical functions for *a*-Se films, detailed measurements of room-temperature normal-incidence transmittance $T_{\exp}(\lambda)$ of undoped *a*-Se films of various thicknesses ($0.25 - 1\ \mu$m) grown by vacuum thermal evaporation on thick glass slides kept at constant temperatures around 30 ℃ were taken as a function of spectral wavelength λ in the range $300 - 1100$ nm. Comprehensive analysis of the as-measured $T_{\exp}(\lambda)$-λ spectra of studied *a*-Se films has been carried out via fitting them to the full theoretical $T_{\text{theor}}(\lambda)$-formulas, combined with differently selected dielectric functions, of an air-supported {thin film/thick substrate}-stacking to determine the spectral dispersion of their optical constants and to realize the nature of light-induced electronic transitions responsible for their experimentally observed optical response.

2. Theoretical Background

An accurate determination of optical constants of a solid film is important both from fundamental and technological viewpoints. The knowledge of the actual dependence of its dielectric functions and optical constants on spectral wavelength (spectral dispersion) enables one to elucidate optical phenomena operative in it and band-energy structure. Further, accurate values of optical constants of solid films are necessary for design and modeling of optoelectronic devices incorporating them. Most optical studies involve measurements on multi-layered structures comprising of solid films made from insulating and semiconducting materials, with the ultimate aim to retrieve spectral dispersion of their optical parameters. One needs first to measure macroscopic optical quantities of a multi-layered structure correlated to the optical parameters of its layers and applicable

theoretical formulas that typify the measured macroscopic optical quantities are then required. A reliable approach is necessary to analyze the as-measured data of such macroscopic optical quantities in view of these respective theoretical formulas. To finalize optical analysis, dielectric and absorption models that would properly describe the spectral behavior of the optical parameters of investigated films will be supportive. As all these issues are of prime concern for the present work, a brief summary on each is given below.

2.1 Measurements and Analytical Techniques for Determining Optical Constants of Solid Films

If a model of a linear, isotropic, homogeneous, dispersive, and uniform non-magnetic lossy solid film with smooth and parallel-plane surfaces (an "*ideal uniform*" film) can be adopted, its optical properties can be completely determined by a *complex* index of refraction $\hat{n}(\lambda) = n(\lambda) + j\,\kappa(\lambda)$ whose real and imaginary parts $n(\lambda)$ and $\kappa(\lambda)$ are, respectively, the normal index of refraction and extinction coefficient of the film, related to its absorption coefficient $\alpha(\lambda)$ as $\kappa(\lambda) \equiv \lambda\,\alpha(\lambda)/4\pi$. Therefore, in principle, two independent optical measurements are necessary at each spectral wavelength λ to solve for the unknowns $n(\lambda)$ and $\kappa(\lambda)$ but, in practice, the true geometric thickness d of the film is not known in prior and is thus to be determined at the same time- that is, three unknowns to be retrieved from two independent optical measurements at the same spectral wavelength, which demands adequate model suppositions or an otherwise optical analytical approach (Tan, 2006; Tan et al., 2007; Tan et al., 2006; Vautier et al., 1988; Bettstelleret al., 1993; Mulama et al., 2014; Benkhedir, 2006; Solieman et al., 2014; Adachi & Kao1980; Kotkata & Abdel-Wahab, 1990; Kotkata et al., 2009; Navarrete et al., 1990; Solieman & Abu-Sehly, 2010; Nagels et al., 1995; Tichy et al., 1996; Nagels et al., 1997; Innami et al., 1999; Tauc, 1972; Tauc, 1979; Heavens, 1991; Azzam & Bashara, 1987; Ward, 1994; Dragoman & Dragoman, 2002; Stenzel, 2005; Joo et al., 1999; Dobrowolski et al., 1983; Klein et al., 1990; Kukinyi et al., 1996; Chiao et al., 1995; Case, 1983; Peng & Desu, 1994; Birgin et al., 1999; Mulato et al., 2000; Erarslan & Gungor, 2010; Ventura et al., 2005; Manifacier et al., 1976; Swanepoel, 1983; Minkov, 1990; El-Naggar et al., 2009; Epstein et al., 1987; González-Leal et al., 1998; Tigau, 2006; Poelman & Smet, 2003). If such film's specifications are, however, not met, as in case of "non-ideal" solid films that suffer from serious inhomogeneities such as surface roughness, compositional inhomogeneity, and thickness non-uniformity, one may adopt additional justifiably harsh model approximations and modifications or employs specific analytical or numerical procedures to model their optical properties, albeit with somewhat more complexity (Swanepoel, 1984; Bennouna et al., 1992; Márquez et al., 1995; Ruíz-Pérez et al., 2001; Márquez et al., 1999; Pradeep & Agarwal, 2010; Richards, 1998; Richards et al., 2004; Theiss, 2012).

The most common, cost-effective, and non-destructive experimental techniques often used to measure macroscopic optical quantities of a solid film or layered structure composing of several films are the spectroscopic ellipsometry (Azzam & Bashara, 1987) and spectrophotometry (Ward, 1994; Dragoman & Dragoman, 2002; Stenzel, 2005), each with its own advantages, limitations, and drawbacks. The latter optical measuring technique, in which we are concerned here, enables one to measure directly the macroscopic specular reflectance $R_{\exp}(\lambda)$ and/or transmittance $T_{\exp}(\lambda)$ of a multi-layered structure integrating such a film over a wide range of spectral wavelengths of the light incident upon the structure; however, the transmittance (or reflectance) is not an *intrinsic* property of the film's material and in general has no direct proportionality to its optical parameters; thus, further quantitative analysis of the $T_{\exp}(\lambda) - \lambda$ and/or reflectance $R_{\exp}(\lambda) - \lambda$ spectra of the film or the structure including the film is needed to determine its geometric thickness as well as its optical constants $n(\lambda)$ and $\kappa(\lambda)$ at each λ, and hence their dispersion functions and electronic transitions responsible for optical absorption in the film.

Many approaches, each with its own limits of applicability, were used to get geometric thickness and optical constants $n(\lambda)$ and $\kappa(\lambda)$ of a solid film from its as-measured $T_{\exp}(\lambda) - \lambda$ and/or $R_{\exp}(\lambda) - \lambda$ spectra. A common approach is the indirect (inverse) synthesis technique $\{T_{\exp}(\lambda),\ R_{\exp}(\lambda)\} \longrightarrow \{\,n(\lambda), \kappa(\lambda)\}$, which is based on inserting multi-constant dispersion function for $n(\lambda)$ and $\kappa(\lambda)$ (Tan, 2006; Tan et al., 2007; Tan et al., 2006; Theiss, 2012; Forouhi & Bloomer, 1986; Forouhi & Bloomer, 1988; Adachi, 1991; Jellison & Modine, 1996; Chambouleyron & Martínez, 2001; Truong & Tanemura, 2006; Kasap & Capper, 2006; Christman, 1988; Rogalski & Palmer, 2000; Palik, 1998; Dressel & Grüner, 2002; Reitz et al., 1993) into theoretical formulas of transmittance and/or reflectance of a multi-layered structure including the film, and then use a powerful statistical curve-fitting program to attain simulated transmittance and reflectance curves to the entire $T_{\exp}(\lambda) - \lambda$ and $R_{\exp}(\lambda) - \lambda$ data (Solieman et al., 2014; Navarrete et al., 1990; Solieman & Abu-Sehly, 2010; Joo et al., 1999; Dobrowolski et al., 1983; Klein et al., 1990; Kukinyi et al., 1996; Chiao et al., 1995; Theiss, 2012). Numeric inversion approaches, armed with dielectric models, are also used for analyzing optical data acquired from spectroscopic ellipsometry, which are based on measured polarized-light reflection quantities of a structure that are directly related its optical functions. In numeric inversion curve-fitting, the film's thickness and constants of selected dispersion relations are treated as adjustable parameters. When a global optimum solution of the fitting problem is realized, the output parameters will be evocative and physically meaningful; otherwise, local multi

solutions are obtained, and hence the output parameters must be identified with utmost care to reject vulnerable ones and select those yield reliable solution, a job that is virtually challenging unless it is assisted by related independent findings.

The Pointwise Unconstrained Minimization Approach (PUMA) numerical method (Birgin et al., 1999; Mulato et al., 2000; Erarslan & Gungor, 2010; Ventura et al., 2005) and algebraic methods (Peng & Desu, 1994; Birgin et al., 1999), based on approximate equations derived from reasonable assumptions, were widely used to extract spectral dispersion of optical constants of a film and its geometric thickness from normal-incidence $T_{\exp}(\lambda)$-λ and/or $R_{\exp}(\lambda)$-λ spectra of its air-supported {thin film/thick substrate}-stack, both of which *do not* require in prior a dispersion functional model. An algebraic method in this category is the *envelope method*, developed and refined by a number of authors (Manifacier et al., 1976; Swanepoel, 1983; Minkov, 1990; El-Naggar et al., 2009; Epstein et al., 1987; González-Leal et al., 1998; Tigau, 2006; Poelman & Smet, 2003), whose viability is based on the presence of many interference-fringe maxima and minima on transmittance (reflectance) spectra in transparent and weak absorption regions of the film, and cannot be applied to spectra displaying few interference fringes. This is not a problem in optical analysis based on PUMA program or curve-fitting softwares that can be used to analyze transmittance and reflectance spectra of multi-layered structures, irrespective of the number of observed interference-fringe extrema. Curve-fitting methods demand multi-constant dispersion formulas, increasing the possibility of obtaining multi local non-global solutions, but, despite of this drawback and the prior need for dielectric models are worldwide, inevitable, and expedient for comprehensive analysis of normal-/obliquely-incidence optical spectra of ideal or non-ideal multi-layered structures incorporating one or more layers over their transparent and absorbing regions, whether displaying interference fringes or not. Curve-fitting procedures are widely allocated in many commercial software programs like, for instant, the SCOUT software, where many dielectric functions and matrix-form theoretical formulations of transmittance and reflectance of multi-layered stacks are installed (Theiss, 2012). We shall utilize to fit as-measured normal-incidence transmittance spectra of our {air/thin *a*-Se film/thick glass substrate/air}-samples to the full respective theoretical formulations of specular transmittance (Swanepoel, 1983; Minkov, 1990; Jafar, 2013).

2.2 Formulations of Normal-Incidence Transmittance and Reflectance of Three-and Four-Layered Structures

We shall quote here the expressions that describe the *normal-incidence* specular transmittance and reflectance of an optically absorbing thick layer standing freely in air (an air-supported *incoherent* layer) and of an ideal air-supported {thin film/thick substrate}-stack. The full theoretical formulations for specular transmittance and reflectance of multi-layered structures at which monochromatic light waves are *obliquely incident* and the mathematical approaches used to derive them are discussed in detail in a variety of scientific reviews and advanced books (Richards, 1998; Chambouleyron & Martínez, 2001; Truong & Tanemura, 2006; Kasap & Capper, 2006; Palik, 1998; Dressel & Grüner, 2002; Reitz et al., 1993; Jackson, 1998; Born & Wolf, 2002; Jafar, 2013; Nichelatti, 2002; Dresselhaus, 2001) and in Appendix A.

2.2.1 An Incoherent Thick Layer Standing Freely in Air

Let monochromatic light beam of wavelength λ and spectral bandwidth (SBW) $\Delta\lambda$ propagating in air is incident normally at a surface of an absorbing slab (s) standing freely in air (an *air-supported three-layered* stack). If the slab has thickness $d_{\rm s}$, smooth, homogenous surfaces, complex index of refraction $\hat{n}_{\rm s}(\lambda) = n_{\rm s}(\lambda) + j\,\kappa_{\rm s}(\lambda)$, and is sufficiently thick (*incoherent*) such that $\Delta\lambda \gg \lambda^2/2\pi n_{\rm s} d_{\rm s}$, light intensities of back and forth light-wave reflections at its internal interfaces with air (v) of $\hat{n}_{\rm v}(\lambda) \cong 1.0 + j\,0$ can be added algebraically (*incoherently*) to give expressions for its specular reflectance $R(\lambda)$ and transmittance $T(\lambda)$ of the form (Richards, 1998; Richards et al., 2004; Theiss, 2012; Chambouleyron & Martínez, 2001; Truong & Tanemura, 2006; Kasap & Capper, 2006; Palik, 1998; Dressel & Grüner, 2002; Reitz et al., 1993; Jackson, 1998; Born & Wolf, 2002; Jafar, 2013; Nichelatti, 2002; Dresselhaus, 2001)

$$T_{\rm vsv}(\lambda) = \frac{(1-R_{\rm vs})^2\left(1+\frac{\kappa_{\rm s}^2}{n_{\rm s}^2}\right)e^{-\alpha_{\rm s}d_{\rm s}}}{1-{\rm R}_{\rm vs}^2\,e^{-2\alpha_{\rm s}d_{\rm s}}} \tag{1}$$

$$R_{\rm vsv}(\lambda) = R_{\rm vs} + \frac{R_{\rm vs}(1-R_{\rm vs})^2\left(1+\frac{\kappa_{\rm s}^2}{n_{\rm s}^2}\right)e^{-2\alpha_{\rm s}d_{\rm s}}}{1-{\rm R}_{\rm vs}^2 e^{-2\alpha_{\rm s}d_{\rm s}}} \tag{2}$$

The slab's absorption coefficient $\alpha_{\rm s}(\lambda)$ is related to its extinction coefficient $\kappa_{\rm s}(\lambda)$ as $\alpha_{\rm s}(\lambda) \equiv 4\pi\kappa_{\rm s}(\lambda)/\lambda$, and the intensity reflection coefficient $R_{\rm vs}$ $(= R_{\rm sv})$ at the vacuum-slab (vs-) interface is given by the formula

$$R_{\rm vs}(\lambda) = \frac{[n_{\rm s}(\lambda)-1]^2+[\kappa_{\rm s}(\lambda)]^2}{[n_{\rm s}(\lambda)+1]^2+[\kappa_{\rm s}(\lambda)]^2} \tag{3}$$

The theoretical $T_{\mathrm{vsv}}(\lambda)$ and $R_{\mathrm{vsv}}(\lambda)$ formulations given in Equations (1) and (2), in conjunction with the expression of $R_{\mathrm{vs}}(\lambda)$ given in Equation (3), can be used in conventional curve-fitting of experimental $T_{\mathrm{exp}}(\lambda)$- λ and $R_{\mathrm{exp}}(\lambda)$- λ spectra of a thick material film (slab) over the entire studied wavelength range, but via insertion of a combination of apt dielectric models (dispersion functions) for its optical constants $n_{\mathrm{s}}(\lambda)$ and $\kappa_{\mathrm{s}}(\lambda)$. An assumption that is viable and justifiable for many dielectric and undoped semiconducting materials is when $\kappa_{\mathrm{s}}^2 \ll n_{\mathrm{s}}^2$, which is true in the transparent and weakly absorbing regions of such substances and is also virtually valid in their strong optical absorption regions. In view of this model approximation, Equations (1) and (2) reduce to simpler analytical forms on the basis of which one can calculate directly, at each spectral wavelength λ, the optical constants $n_{\mathrm{s}}(\lambda)$ and $\kappa_{\mathrm{s}}(\lambda)$ or $\alpha_{\mathrm{s}}(\lambda)$ of an air-supported thick dielectric or semiconducting slab from the measured values of its $T_{\mathrm{exp}}(\lambda)$ and $R_{\mathrm{exp}}(\lambda)$ (Nichelatti, 2002). Both of the aforesaid optical analytical approaches are useful when a thick slab is used as a substrate on which a thin film of absorbing material is deposited, as one can model the optical constants of this substrate and insert the obtained results in theoretical formulas describing the optical response of a multi-layered structure containing the film.

2.2.2 An Air-Supported Stack of a Coherent Thin Film Placed on an Incoherent Thick Substrate

Consider a simple and ideal *four-layered* structure having the {air/thin film/thick substrate/air}-stack- that is, an air-supported {film-substrate}-system at which monochromatic light of wavelength λ and SBW $\Delta\lambda$ is *normally incident* at the air (v)-film (f) interface. Let the substrate and film to have complex indices of refraction $\hat{n}_{\mathrm{s}}(\lambda) = n_{\mathrm{s}}(\lambda) + j\,\kappa_{\mathrm{s}}(\lambda)$ and $\hat{n}(\lambda) = n(\lambda) + j\,\kappa(\lambda)$, respectively, and film's geometric thickness d is amply small such that $\Delta\lambda \ll \lambda^2/2\pi nd$ with smooth, homogeneous, and plane-parallel surfaces- that is, a *coherent ideal thin film*; thus, multiple internal light-wave reflections inside it and interference between them will be both important. If the substrate (s) has a *finite incoherent* geometric thickness d_{s} ($\gg d$), only multiple internal light plane wave reflections inside it are significant, but not interference between the reflected/transmitted waves. We shall quote only the theoretical expression that describes the specular transmittance $T_{\mathrm{vfsv}}(\lambda)$ of this ideal {air/thin film/thick substrate/air}-structure for the normally-incident monochromatic light waves propagating along the vfsv-*route*, which can be written in the form (Minkov, 1990; Jafar, 2013)

$$T_{\mathrm{vfsv}}(\lambda) = \frac{(\tau_{\mathrm{vf}}^2\,\tau_{\mathrm{fs}}^2\,e^{-\alpha d})(\,\tau_{\mathrm{sv}}^2\,e^{-\alpha_{\mathrm{s}} d_{\mathrm{s}}})}{1-\frac{\rho_{\mathrm{fs}}^2+\rho_{\mathrm{vf}}^2\,e^{-2\alpha d}+2\rho_{\mathrm{vf}}\,\rho_{\mathrm{fs}}\,e^{-\alpha d}\cos\left(2\delta_{\mathrm{f}}'+\phi_{\mathrm{vf}}-\phi_{\mathrm{fs}}\right)}{1+\rho_{\mathrm{vf}}^2\,\rho_{\mathrm{fs}}^2\,e^{-2\alpha d}+2\rho_{\mathrm{vf}}\,\rho_{\mathrm{fs}}\,e^{-\alpha d}\cos\left(2\delta_{\mathrm{f}}'+\phi_{\mathrm{vf}}+\phi_{\mathrm{fs}}\right)}(\rho_{\mathrm{sv}}^2 e^{-2\alpha_{\mathrm{s}} d_{\mathrm{s}}})} \tag{4}$$

where ρ_{lm} and τ_{lm} are, respectively, the *real scalar reflection* and *transmission* coefficients at the interfaces of adjacent l-m layers of this ideal four-layered structure, while ϕ_{lm} are the related phase-change angles produced upon wave reflections at the l-m interfaces, which for *normal incidence* are given by the expressions (Minkov, 1990; Born & Wolf, 2002; Jafar, 2013)

$$\rho_{lm}^2 \equiv \frac{(n_l-n_m)^2+(\kappa_l-\kappa_m)^2}{(n_l+n_m)^2+(\kappa_l+\kappa_m)^2} \tag{5}$$

$$\tan\phi_{lm} = -\frac{2\,(n_l\kappa_m-n_m\kappa_l)}{(n_l^2+\kappa_l^2)-(n_m^2+\kappa_m^2)} \tag{6}$$

$$\tau_{lm}^2 \equiv \frac{4\,(n_l^2+\kappa_l^2)}{(n_l+n_m)^2+(\kappa_l+\kappa_m)^2} \tag{7}$$

where $\alpha \equiv 4\pi\kappa/\lambda$ and $\alpha_{\mathrm{s}} \equiv 4\pi\kappa_{\mathrm{s}}/\lambda$ are absorption coefficients of film and substrate, respectively, and $\hat{\delta}_{\mathrm{f}} \equiv \delta_{\mathrm{f}}' + j\,\delta_{\mathrm{f}}'' = (2\pi nd/\lambda) + j(2\pi\kappa d/\lambda) = (\varphi/2) + j(\alpha\,d/2)$ is the *normal-incidence complex phase-change* angle produced upon a *single traversal* of light waves inside the *coherent thin film*, with φ being the associated interference phase-change angle (Minkov, 1990; Born & Wolf, 2002; Jafar, 2013). For purposes of analyzing the experimental transmittance data of an air-supported {film-substrate}-stack, all the real scalar reflection and transmission coefficients and related phase-change angles entering in the $T_{\mathrm{vfsv}}(\lambda)$-formula given in equation (4) are expressed in terms of real and imaginary parts of complex indices of refraction of film and substrate (n, κ, n_{s}, and κ_{s}). The resulting theoretical $T_{\mathrm{vfsv}}(\lambda)$-formula will be inconvenient for algebraic analytical handling of as-measured $T_{\mathrm{exp}}(\lambda)$ at a wavelength λ and the $T_{\mathrm{exp}}(\lambda)$- λ spectrum can only be analyzed by a curve-fitting technique to fit it to the $T_{\mathrm{vfsv}}(\lambda)$-formula, with the effect of optical absorption in both film and substrate can be taken into account over the entire spectral range studied. Yet, the optical functions of a substance are not in general constants but vary with wavelength (dispersive), so the problem will be much elaborate and dispersion functions will be needed to describe them. So, many constant parameters will be adjusted in the process of data curve-fitting, which would add to the number of local-minima multiple solutions with different and unrealistic

outputs. Only when a global minimum solution for the curve-fitting problem is achieved, one obtains reliable and informative dielectric and optical parameters for the studied film. If the substrate in the {air/thin uniform film/thick substrate/air}-stacking is transparent ($\kappa_s \cong 0$) in the spectral region above the absorption edge of the film, the $T_{\mathrm{vfsv}}(\lambda)$-formula given in Equation (4) reduces to a wieldy expression that forms the basis of the analytical envelope and PUMA methods (Birgin et al., 1999; Mulato et al., 2000; Erarslan & Gungor, 2010; Ventura et al., 2005; Manifacier et al., 1976; Swanepoel, 1983; Minkov, 1990; El-Naggar et al., 2009; Epstein et al., 1987; González-Leal et al., 1998; Tigau, 2006; Poelman & Smet, 2003; Swanepoel, 1984; Chambouleyron & Martínez, 2001; Truong & Tanemura, 2006; Kasap & Capper, 2006), the application of which do not necessitate in prior dispersion functions for the film's optical constants.

2.3 Dielectric and Optical Functions for Dielectric and Semiconducting Substances

Polar solids contain intrinsic electric dipoles with net permanent moments, ionic solids consist of positive and negative charges (ions), and metals or doped semiconductors are rich in free electrons (holes), and all consist of atoms (nuclei plus valence and core bound electrons). Classically, electrons and nuclei of atoms in dielectrics and undoped semiconductors as well as ion pairs in ionic substances are visualized to be pushed apart (slightly) by the force caused by a weak externally applied electrostatic field; thus, forming a collection of microscopic electric dipoles, the resultant of which gives rise to a net electric dipole moment or macroscopic polarization inside the sample- that is, the sample becomes electrically polarized. The permanent electric dipoles in a polar solid, however, are more or less free to rotate and will be re-oriented under the action of both of the applied electric field and thermal agitations, with the resulting orientational electric polarization being strongly dependent on ambient temperature of the polar solid, whereas the field-induced shifts of electrons bounded to its atoms relative to their respective nuclei result in a temperature-independent electronic (deformation) polarization (Tan, 2006; Tan et al., 2007; Tan et al., 2006; Chambouleyron & Martínez, 2001; Truong & Tanemura, 2006; Kasap & Capper, 2006; Christman, 1988; Rogalski & Palmer, 2000; Palik, 1998; Dressel & Grüner, 2002; Reitz et al., 1993; Jackson, 1998; Born & Wolf, 2002). On the contrary, response of a metal under the action of an electrostatic field is quite different and electrons (holes) are envisioned to be expelled out of its interior.

In the presence of an external *time-dependent* weak electric field, oppositely-charged ions and electrons bounded to atoms in a dielectric will, however, oscillate in response as the time-dependent electric field acting at their positions $\mathbf{r}$ inside it- that is- as the local electric field $\boldsymbol{\mathcal{E}}_{\mathrm{loc}}(\mathbf{r},t)$. The oscillatory motion of electric dipoles due to electromagnetic field-induced shifts of ion pairs or distortions of electronic charge distribution around nuclei can be pictured by their time-dependent microscopic electric polarizabilities, the overall effect of which revealed itself in a macroscopic dielectric behavior of the radiation-excited sample, exemplified in terms of its frequency-dependent macroscopic complex electric susceptibility $\hat{\chi}(\omega) \equiv \chi'(\omega) + j\chi''(\omega)$ or complex dielectric constant $\hat{\epsilon}(\omega)$ as $\hat{\chi}(\omega) \equiv \hat{\epsilon}(\omega) - 1$ or complex index of refraction $\hat{n}(\omega) \equiv n(\omega) + j\kappa(\omega) = \sqrt{\hat{\epsilon}(\omega)}$. Note that the real and imaginary parts of $\hat{\chi}(\omega)$, $\hat{\epsilon}(\omega)$, and $\hat{n}(\omega)$ are interrelated via their respective fundamental Kramers-Kronig (KK) integral relations (Palik, 1998; Dressel & Grüner, 2002; Reitz et al., 1993; Jackson, 1998; Born & Wolf, 2002).

Accurate description of field-induced distortion of electronic charge distribution around atoms or shifts of ion pairs in a solid can be skilled via quantum-mechanical formulation in the electric dipole approximation and time-dependent perturbation theory (Rogalski & Palmer, 2000; Palik, 1998; Dressel & Grüner, 2002; Dresselhaus, 2001; Bassani & Parravicini, 1975; Sólyom, 2009). However, both classical and quantum-mechanical treatments of the problem yield similar concluding results, but sometimes quantum-mechanical treatment is inevitable, as when one wishes to reveal the nature and features of band-to-band optical absorption processes in the solid that are related to its energy band structure. Details of the various approaches adopted in classical- and quantum-mechanical treatments of the radiation-induced dielectric and optical response of dielectrics and conducting materials (metals and doped semiconductors) can be found in a number of literature reports and advanced books of electrodynamics and solid-state physics (Tauc, 1972; Tauc, 1979; Heavens, 1991; Azzam & Bashara, 1987; Ward, 1994; Dragoman & Dragoman, 2002; Stenzel, 2005; Theiss, 2012; Forouhi & Bloomer, 1986; Forouhi & Bloomer, 1988; Adachi, 1991; Jellison & Modine, 1996; Chambouleyron & Martínez, 2001; Truong & Tanemura, 2006; Kasap & Capper, 2006; Christman, 1988; Rogalski & Palmer, 2000; Palik, 1998; Dressel & Grüner, 2002; Reitz et al., 1993; Jackson, 1998; Dresselhaus, 2001; Bassani & Parravicini, 1975; Sólyom, 2009).

The formulations that describe frequency dependence of dielectric and optical functions of linear, isotropic, and non-magnetic dielectrics and semiconductors can be derived in the frame of a classical handling of the problem based on the linearity and causality of its time-dependent electric response, where constitutive formulas relating a time-dependent macroscopic electric polarization vector $\mathbf{P}(\mathbf{r},t)$ or displacement vector $\mathbf{D}(\mathbf{r},t) \equiv \epsilon_0\mathbf{E}(\mathbf{r},t) + \mathbf{P}(\mathbf{r},t)$ to the exciting electromagnetic field $\mathbf{E}(\mathbf{r},t)$ have no physical meaning (Palik, 1998; Dressel & Grüner,

2002; Reitz et al., 1993; Jackson, 1998; Dresselhaus, 2001; Bassani & Parravicini, 1975; Sólyom, 2009). There is no electric susceptibility $\chi(t)$ of a material in the time domain that linearly relates $\mathbf{P}(\mathbf{r},t)$ to externally-exciting electric field $\mathbf{E}(\mathbf{r},t)$; electric susceptibility is, however, a frequency-domain physical property of material. For a linear, isotropic, dispersive, and lossy sample, $\hat{\chi}(\omega)$ and $\hat{\epsilon}(\omega)$ $(\equiv \hat{\chi}(\omega)+1)$ are complex Fourier inverse transform response functions that correspond to its time-dependent response functions $\chi(t)$ and $\epsilon(t)$ (Reitz et al., 1993; Jackson, 1998) and fulfill linear constitutive relations $\hat{P}(\omega) \equiv \epsilon_0\hat{\chi}(\omega)\hat{E}(\omega)$ and $\hat{D}(\omega) \equiv \epsilon_0\hat{\epsilon}(\omega)\hat{E}(\omega)$, where ϵ_0 is free-space permittivity. Assume that the sample is exposed to weak electromagnetic radiations with ultraviolet frequencies and below, so their wavelengths are much larger than interatomic spacing and diffraction features are unimportant, and $\boldsymbol{\mathcal{E}}_{\mathrm{loc}}(\mathbf{r},t)$ at the site of a field-induced electric dipole is linearly connected to the macroscopic electric field $\boldsymbol{\mathcal{E}}_{\mathrm{mac}}(\mathbf{r},t)$ inside the substance. For linear, isotropic, and highly-symmetric crystalline and amorphous non-polar dielectric solids, we have $\boldsymbol{\mathcal{E}}_{\mathrm{loc}}(\mathbf{r},t) \cong \boldsymbol{\mathcal{E}}_{\mathrm{mac}}(\mathbf{r},t) + \mathbf{P}(\mathbf{r},t)/3\epsilon_0$ (Kasap & Capper, 2006, Christman, 1988; Rogalski & Palmer, 2000; Palik, 1998; Dressel & Grüner, 2002; Reitz et al., 1993; Jackson, 1998). Quantum-mechanical formulations and physics of dielectric and absorption phenomena related to radiation-induced direct and indirect band-to-band (interband) electronic transitions in crystalline substances are presented in Appendix B. Formulations of a forced-damped Lorentz harmonic oscillator dispersion model that describe dielectric and optical response of electrons bounded to atoms of linear, isotropic, and non-magnetic dielectrics exposed to electromagnetic fields are given below. The physics features and formulations of dielectric models used to analyze optical response of crystalline and amorphous semiconductors in the absorption edge (interband) and sub-bandgap regions will then be briefed.

2.3.1 Forced-Damped Lorentz Harmonic Oscillator Dielectric Model

Optical response of a dielectric sample of N atoms, each of Z bound electrons, as a function of angular frequency ω (wavelength λ) of incident light can be discussed on the basis of a forced-damped harmonic (Lorentz) oscillator model. A common oscillator-like $\hat{\epsilon}(\omega)$-formulation for a collection of N non-interacting atoms (zero Lorentz field-correction factor) for a group of Lorentz oscillators with diverse resonance frequencies ω_{0i}, quantum-mechanical strengths f_{0i} $(\sim \omega_{0i})$ with $\sum_i f_{0i} = Z$, and damping frequencies (broadening linewidths) γ_i is given by (Navarrete et al., 1990; Innami et al., 1999; Tauc, 1972; Tauc, 1979; Heavens, 1991; Azzam & Bashara, 1987; Ward, 1994; Dragoman & Dragoman, 2002; Stenzel, 2005; Poelman & Smet, 2003; Adachi, 1991; Jellison & Modine, 1996; Chambouleyron & Martínez, 2001; Truong & Tanemura, 2006; Kasap & Capper, 2006; Christman, 1988; Rogalski & Palmer, 2000; Palik, 1998; Dressel & Grüner, 2002; Reitz et al., 1993; Jackson, 1998; Born & Wolf, 2002; Dresselhaus, 2001; Bassani & Parravicini, 1975; Sólyom, 2009)

$$\hat{\epsilon}(\omega) = \epsilon'(\omega) + j\epsilon''(\omega) = \epsilon_\infty + \sum_i \frac{\omega_{\mathrm{p}}^2 f_{0i}}{\omega_{0i}^2 - \omega^2 - j\gamma_i\omega} = \epsilon_\infty + \sum_i \frac{\bar{\nu}_{\mathrm{p}i}^2}{\bar{\nu}_{0i}^2 - \bar{\nu}^2 - j\bar{\nu}_{ti}\bar{\nu}} \tag{8}$$

where $\omega_p = \sqrt{Ne^2/m^*\epsilon_0}$ is the plasma frequency, with e and m^* being, respectively, the magnitude of electronic charge and effective mass of the electron in the solid. The wavenumbers $\bar{\nu}$ $(= 1/\lambda = \omega/2\pi c)$, $\bar{\nu}_{0i}$ $(= 1/\lambda_{0i} = \omega_{0i}/2\pi c)$, and $\bar{\nu}_{ti}$ $(= 1/\lambda_{ti} = \gamma_i/2\pi c)$ are introduced to reconcile with numeric curve-fitting procedures being adopted in the present work, with the energy values in eV units can be found by dividing the values of respective wavenumbers (in cm^{-1}) by the number 8065. The parameter ϵ_∞ is a dielectric constant that is introduced, instead of 1 in standard form of Lorentz oscillator model (Navarrete et al., 1990; Poelman & Smet, 2003; Jellison & Modine, 1996). For a linear, isotropic, and non-magnetic lossy dielectric, the optical constants $n(\lambda)$ and $\kappa(\lambda)$ can readily be evaluated from the relations $\epsilon'(\omega) = n^2 - \kappa^2$ and $\epsilon''(\omega) = 2n\kappa$.

A sum of two Lorentz oscillators with diverse resonance frequencies ω_{0i}, quantum-mechanical strengths f_{0i} $(\sim \omega_{0i})$ with $\sum_i f_{0i} = Z$, and damping frequencies (broadening linewidths) γ_i has been used to describe complex dielectric constant function $\hat{\epsilon}(\omega)$ of undoped *a*-Se films (Navarrete et al., 1990). However, dispersion formulations that integrate only multi-Lorentz harmonic oscillators would be unsatisfactory to account for optical behavior of a semiconducting sample in the region of its absorption edge (interband transition region), since all energy states in its valence and conduction bands separated in energy by the exciting photon energy $\hbar\omega$ are involved in radiation-induced electronic transitions and many adjustable fitting parameters are required for a comprehensive analysis of its optical data over a wide spectral range on the basis of Lorentz model only. So, one needs other dispersion models which takes into consideration possible contributions to dielectric and optical response of a semiconducting solid film over a wide range of photon energies that cover its band-to-band (interband) and sub-bandgap energy regions. Further, these dielectric models should also have closed analytical forms that will be virtually convenient and computationally feasible for analyzing experimental optical data of non-crystalline solids, but with few parameters of physical significance. Some of the currently available and operational dispersion and optical absorption models that lie in this category will now be briefed.

2.3.2 Band-to-Band (Interband) Transition Models for Amorphous Dielectrics and Semiconductors

Laboratory fabricated dielectric and semiconducting films are widely integrated in the construction of technological and electronic devices; however, as-produced films normally suffer from inhomogeneity and structural disorders, so containing significant number of inherent (native) defects and imperfections, in addition to intrinsic (native) impurities initially present in starting ingots used in fabrication. The existence of native defects in solids leads to a destruction in their crystallinity via eradicating the long-range positional and orientational periodicity of their atoms; thus, such films are termed disordered amorphous, where structural crystallinity prevails over only short-range regions. The lack of a long-range order structure and deficit lattice periodicity in amorphous samples makes Bloch theorem inapplicable for them and crystalline wavevector (momentum) undefined, with complicated and ambiguous energy band structures. However, it is well known that the valence and conduction bands retain their meaning even in the amorphous state and locally the electronic states in an amorphous solid may be considered to be a broadened superposition of molecular-orbital sates. In tetrahedrally-coordinated and chalcogenide amorphous materials like amorphous selenium (*a*-Se), linear combinations of atomic (molecular) orbitals lead to bonding, nonbonding, and antibonding molecular states which then broaden into a series of separated valence and conduction bands when the solid is formed, the contributions of which in an amorphous sample to its dielectric and absorption processes often render its macroscopic optical absorption and reflection spectra to display a single broad peak (Innami et al., 1999; Tauc, 1979; Adachi, 1991).

The short-range-ordered energy states in undoped *a*-Se produce five local valence and conduction bands (Innami et al., 1999): an upper conduction band (UCB) formed essentially from atomic *s*-states, a lower conduction band (LCB) set of antibonding atomic *p*-states, an upper valence band (UVB), associated with nonbonding (lone pair) atomic *p*-states of selenium, a midvalence band (MVB) set of bonding atomic *p*-states, and a lower valence band (LVB). The LVB is narrow, and the threshold energy for exciting its *s*-electrons to a conduction band is very high; thus, one could treat these electrons as core electrons. A broad absorption spectrum of an undoped *a*-Se solid film will comprise of only four overlapping absorption peaks when optical measurements are made over a wide spectral range, and such absorption peaks are related to $\mathrm{UVB} \rightarrow \mathrm{LCB}$ ($E_{\mathrm{g1}} \sim 1.87\ \mathrm{eV}$), $\mathrm{MVB} \rightarrow \mathrm{LCB}$ ($E_{\mathrm{g2}} \sim 2.1\ \mathrm{eV}$), $\mathrm{UVB} \rightarrow \mathrm{UCB}$ ($E_{\mathrm{g3}} \sim 5.5\ \mathrm{eV}$), and $\mathrm{MVB} \rightarrow \mathrm{UCB}$ ($E_{\mathrm{g4}} \sim 5.78\ \mathrm{eV}$) electronic transitions with threshold bandgap energies E_{gi} (i =1, 2, 3, and 4), all of which contribute to its optical response (Innami et al., 1999). Structural disorder in a semiconducting sample leads to the formation of localized energy states in the energy bandgap (band tails), which further contribute to its optical response. This implies that dielectric and optical properties of an amorphous film are unlike those of a crystal made from same material, and hence parameterization of its optical functions will be different. However, an understanding of optical response of amorphous materials exposed to electromagnetic radiation may be achieved if analytical relations of dispersion processes and optical absorption in crystalline materials are modified to suit amorphous counterparts.

There is yet no single dielectric relation viable in a wide range of wavelengths covering interband transition and sub-bandgap regions of even a perfect crystal, as several dielectric and absorption processes contribute differently to its optical response in different spectral regions. Further, a complete theory that describes unambiguously optical response of crystalline materials is quite tangled and is not well developed in real world. It is a habit to treat independently a sample's response in different wavelength ranges to find matching dielectric functions and combine them to describe its overall response. The physics and theoretical formulas that describe optical behavior of crystalline materials in the absorption edge and sub-bandgap regions are discussed in literature (Tan, 2006; Tan et al., 2007; Tan et al., 2006; Innami et al., 1999; Tauc, 1972; Tauc, 1979; Heavens, 1991; Azzam & Bashara, 1987; Ward, 1994; Dragoman & Dragoman, 2002; Stenzel, 2005; Joo et al., 1999; Poelman & Smet, 2003; Theiss, 2012; Forouhi & Bloomer, 1986; Forouhi & Bloomer, 1988; Adachi, 1991; Jellison & Modine, 1996; Chambouleyron & Martínez, 2001; Truong & Tanemura, 2006; Kasap & Capper, 2006; Christman, 1988; Rogalski & Palmer, 2000; Palik, 1998; Dressel & Grüner, 2002; Reitz et al., 1993; Dresselhaus, 2001; Bassani & Parravicini, 1975; Sólyom, 2009; O'Leary et al., 1997; Dias da Silva et al., 2004; Liang & Beal, 1976) and Appendix B, the most common of which that can be modified to discuss optical response of amorphous undoped semiconductors are briefed below.

2.3.2.1 Interband Transition Models for Crystalline Dielectrics and Semiconductors

Let a defect-free, crystalline *direct-band* dielectric or undoped semiconductor to be illuminated by light of an angular frequency ω and photon propagation wavevector $\mathbf{k}_{ph}$. No light absorption will take place in this crystalline sample for photon energies $\hbar\omega < E_{\mathrm{g0}} = E_{\mathrm{c}}(\mathbf{k}=0) - E_{\mathrm{v}}(\mathbf{k}=0)$, which is often referred to as its *fundamental absorption edge* or the minimum energy separation between the maximum point in the valence band (an occupied initial state, $|i\rangle$) and a minimum point in the conduction band (an empty final state, $|f\rangle$)

lying above it at $\mathbf{k} = 0$. The conservation (selection) rule for the total interaction energy of the photon-electron system is not satisfied for low photon energies, though its momentum (wavevector) is conserved ($\mathbf{k}_f \cong \mathbf{k}_i$, as $\mathbf{k}_{ph} \ll \mathbf{k}_i, \mathbf{k}_f$). For $\hbar\omega < E_{g0}$, the imaginary part $\epsilon''(\omega)$ of the complex dielectric constant $\hat{\epsilon}(\omega) \equiv \epsilon'(\omega) + j\epsilon''(\omega)$ or absorption coefficient $\alpha(\omega) \equiv (\omega\,\epsilon''(\omega)/n(\omega)c)$ of a crystalline direct-bandgap semiconductor vanishes (i.e., $\epsilon''(\omega) = \alpha(\omega) = 0$), where $n(\omega)$ is its index of refraction and c is speed of light in vacuum. For $\hbar\omega \geq E_{g0}$, however, all radiation-induced "vertical" (direct) $\mathbf{k}_i \rightarrow \mathbf{k}_f$ electronic excitations occur between occupied and empty energy states in valence and conduction bands separated in energy by $E_c(\mathbf{k}) - E_v(\mathbf{k}) = \hbar\omega$, including those at $\mathbf{k} = 0$. Here, the total energy and momenta of the electron-photon system are both fulfilled, giving rise to a sharp decline in its absorption spectrum in the region of its fundamental absorption edge. Closed-form analytical dielectric formulas for abrupt radiation-induced *direct interband* transitions in a crystalline sample between energy states of wavevector $\mathbf{k}$ in its valence and conduction bands, separated by $\hbar\omega$, can be found from quantum-mechanics description of imaginary part $\epsilon''(\omega)$ of its transverse complex dielectric constant in terms of the *joint-density-of-states* (JDOS) $\mathcal{J}_{cv}(\hbar\omega)$ and optical momentum transition matrix element $\mathbf{M}_{cv}(\mathbf{k})$ (Forouhi & Bloomer, 1986; Forouhi & Bloomer, 1988; Adachi, 1991; Jellison & Modine, 1996; Bassani & Parravicini, 1975; Sólyom, 2009; O'Leary et al., 1997; Dias da Silva et al., 2004; Liang & Beal, 1976). The JDOS $\mathcal{J}_{cv}(\hbar\omega)$ is understood as a combined density of pair of energy states in valence and conduction bands involved in electronic transitions- one occupied and the other empty, separated in energy by $\hbar\omega$. Quantum-mechanical closed analytical form of $\epsilon''(\omega)$ or $\alpha(\omega)$, which determines optical absorption in a perfectly crystalline direct-bandgap semiconductor in its interband transition region, is often expressed (in MKS units) as (Dresselhaus, 2001; Bassani & Parravicini, 1975; Sólyom, 2009; O'Leary et al., 1997; Dias da Silva et al., 2004; Liang & Beal, 1976)

$$\epsilon''(\omega) \equiv \frac{c\,n(\omega)\alpha(\omega)}{\omega} = \frac{e^2}{\epsilon_0 m_e^{*2}\omega^2}\sum_{v,c}\int \frac{2d^3\mathbf{k}}{(2\pi)^3}|\hat{\boldsymbol{e}}.\mathbf{M}_{cv}(\mathbf{k})|^2\,\delta(E_c(\mathbf{k}) - E_v(\mathbf{k}) - \hbar\omega)$$

$$= \frac{e^2}{\epsilon_0 m_e^{*2}\omega^2}\sum_{v,c}|\hat{\boldsymbol{e}}.\mathbf{M}_{cv}(\mathbf{k})|^2\,\mathcal{J}_{cv}(\hbar\omega) = \frac{e^2\hbar^2}{\epsilon_0 m_e^{*2}\omega^2}\sum_{v,c}|\langle c,\mathbf{k}|\hat{\boldsymbol{e}}.\boldsymbol{\nabla}_{\mathbf{k}}|v,\mathbf{k}\rangle|^2\,\mathcal{J}_{cv}(\hbar\omega) \quad (9)$$

The integral extends over all allowed **k**-states in the first Brillouin zone, the factor 2 arises from the two possible electron spins, and m_e^* is the effective mass of electron in the solid, governed by the energy structure of its valence band involved in the interband electronic transitions. Use the Kramers-Kronig dispersion $\epsilon'(\omega)$ -relation, $\epsilon''(\omega)$ -formula of Equation (9) and formalism of Dirac delta function to get the quantum-mechanical $\epsilon'(\omega)$-expression

$$\epsilon'(\omega) = 1 + \frac{2}{\pi}\mathcal{P}\int_0^\infty \frac{\omega'\epsilon''(\omega')}{\omega'^2 - \omega^2}\,d\omega'$$

$$= 1 + \frac{2}{\pi}\left(\frac{e^2}{\epsilon_0 m_e^{*2}}\right)\sum_{v,c}\int \frac{2d^3\mathbf{k}}{(2\pi)^3}\frac{|\hat{\boldsymbol{e}}.\mathbf{M}_{cv}(\mathbf{k})|^2}{\{[E_c(\mathbf{k}) - E_v(\mathbf{k})]/\hbar\}*\{([E_c(\mathbf{k}) - E_v(\mathbf{k})]^2/\hbar^2) - \omega^2\}} \quad (10)$$

The macroscopic $\epsilon'(\omega)$- and $\epsilon''(\omega)$- dielectric functions as well as the macroscopic optical functions satisfy some general relations (called sum rules), which are often used to test the consistency of the approximations involved in their computation and measurements (Dresselhaus, 2001; Bassani & Parravicini, 1975; Sólyom, 2009). The expression for the joint density of states (JDOS) $\mathcal{J}_{cv}(\hbar\omega)$ of all pairs of energy states in valence and conduction bands involved in the direct interband transitions and separated in energy by $E_c(\mathbf{k}) - E_v(\mathbf{k}) = \hbar\omega$ can be illustrated in a general expression having the integral form given below (Bassani & Parravicini, 1975; Sólyom, 2009; O'Leary et al., 1997; Dias da Silva et al., 2004; Liang & Beal, 1976)

$$\mathcal{J}_{cv}(\hbar\omega) \equiv \int \frac{2d^3\mathbf{k}}{(2\pi)^3}\,\delta(E_c(\mathbf{k}) - E_v(\mathbf{k}) - \hbar\omega) = \frac{2}{(2\pi)^3}\int \frac{dS_{\mathbf{k}}}{|\boldsymbol{\nabla}_{\mathbf{k}}[E_c(\mathbf{k}) - E_v(\mathbf{k})]|} \quad (11)$$

where $dS_{\mathbf{k}}$ represents an infinitesimal area element in **k**-space for all possible transitions on the constant-energy surface defined by $E_c(\mathbf{k}) - E_v(\mathbf{k}) = E = \hbar\omega$, with the integral can be evaluated if the energy structures of valence and conduction bands involved in interband transitions are known. The JDOS shows strong variations in the vicinity of specific values of energy E (critical-points), where singularities in the JDOS (van-Hove singularities) and hence in $\epsilon''(\omega)$-spectra occur when $\boldsymbol{\nabla}_{\mathbf{k}}E_c(\mathbf{k}) - \boldsymbol{\nabla}_{\mathbf{k}}E_v(\mathbf{k}) = 0$ at any $\mathbf{k}$ vector (Dresselhaus, 2001; Bassani & Parravicini, 1975; Sólyom, 2009). For an undoped semiconductor at low temperatures where we can assume independent conduction- and valence- band potential fluctuations, the JDOS function may also be expressed by a *convolution integral form* involving the product of the density of states

(DOS) in the conduction band $\mathrm{g_c}(E^*)$ with energy E^* and DOS in the valence band $\mathrm{g_v}(\hbar\omega - E^*)$, taking into account all possible optical transitions between states separated in energy by the exciting photon energy $\hbar\omega$, as described below (Forouhi & Bloomer, 1986; Forouhi & Bloomer, 1988; Adachi, 1991; Jellison & Modine, 1996; O'Leary et al., 1997; Dias da Silva et al., 2004; Liang & Beal, 1976)

$$\mathcal{J}_{\mathrm{cv}}(\hbar\omega) = \int_{-\infty}^{\infty} \mathrm{g_c}(E^*)\, \mathrm{g_v}(\hbar\omega - E^*) dE^* = \int_{-\infty}^{\infty} \mathrm{g_c}(E^* + \hbar\omega)\, \mathrm{g_v}(E^*) dE^* \tag{12}$$

To find a closed analytical form for the frequency dependency of $\epsilon''(\omega)$ and $\epsilon'(\omega)$ of a crystalline semiconductor, we need to calculate the momentum transition matrix element $\mathbf{M}_{\mathrm{cv}}(\mathbf{k})$ of electron-photon interaction Hamiltonian, which is dependent on band structures of its valence and conduction bands involved in the radiation-induced electronic transitions, which for direct interband transitions between energy states of similar wavevectors $\mathbf{k}$ of valence and conduction bands of a three-dimensional (3D) crystalline solid of volume $V = \int d^3\mathbf{r}$ is expressed by an integral of the form (Dresselhaus, 2001; Bassani & Parravicini, 1975; Sólyom, 2009)

$$\hat{\boldsymbol{e}}.\mathbf{M}_{\mathrm{cv}}(\mathbf{k}) = \langle \psi_{\mathbf{ck}} | \hat{\boldsymbol{e}}.\mathbf{p} | \psi_{\mathbf{vk}} \rangle = \langle \psi_{\mathbf{ck}} | \hat{\boldsymbol{e}}.(-j\hbar\boldsymbol{\nabla}_{\mathbf{k}}) | \psi_{\mathbf{vk}} \rangle = \hat{\boldsymbol{e}}. \int \psi_{\mathrm{c}}^*(\mathbf{k},\mathbf{r})\, (-j\hbar\boldsymbol{\nabla}_{\mathrm{cv}})\, \psi_{\mathrm{v}}(\mathbf{k},\mathbf{r}) d^3\mathbf{r} \tag{13}$$

For *allowed direct interband* transitions, the square averaged momentum transition matrix element $|\hat{\boldsymbol{e}}.\mathbf{M}_{\mathrm{cv}}(\mathbf{k})|^2$ between valence and conduction bands is taken to be smooth slowly function of $\mathbf{k}$, but at points near special $\mathbf{k}$ vectors where $\hat{\boldsymbol{e}}.\mathbf{M}_{\mathrm{cv}}(\mathbf{k})$ vanishes because of symmetry, so $\hat{\boldsymbol{e}}.\mathbf{M}_{\mathrm{cv}}(\mathbf{k})$ is assumed to be *constant*, independent of $|\mathbf{k}|$, whereas $|\hat{\boldsymbol{e}}.\mathbf{M}_{\mathrm{cv}}(\mathbf{k})|^2$ varies quadratically in $\mathbf{k}$ for *forbidden direct interband* transitions (Tauc, 1972; Tauc, 1979; Heavens, 1991; Azzam & Bashara, 1987; Ward, 1994; Dragoman & Dragoman, 2002; Stenzel, 2005; Forouhi & Bloomer, 1986; Forouhi & Bloomer, 1988; Adachi, 1991; Jellison & Modine, 1996; Chambouleyron & Martínez, 2001; Truong & Tanemura, 2006; Kasap & Capper, 2006; Christman, 1988; Rogalski & Palmer, 2000; Palik, 1998; Dressel & Grüner, 2002; Dresselhaus, 2001; Bassani & Parravicini, 1975; Sólyom, 2009). To get the frequency dependence of JDOS function $\mathcal{J}_{\mathrm{cv}}(\hbar\omega)$, we need to know the detailed structure of valence and conduction energy bands involved in transitions of electrons between their energy states separated by an energy $\hbar\omega$, as is evident from Equations (11) and (12). If energy states in valence and conduction bands between which radiation-induced electronic transitions taking place in a defect-free crystalline undoped semiconductor of absorption edge E_{g0} are expressed in terms of *parabolic-like* functions in the wavevector $\mathbf{k}$ in the vicinity of their extrema. The contribution of a pair of interband transitions to the frequency variation of $\epsilon''(\hbar\omega)$ with $\hbar\omega$ is proportional to $1/\omega^2$ and to the frequency-dependent $\mathcal{J}_{\mathrm{cv}}(\hbar\omega)$, which can also be shown to be proportional to $\left(\hbar\omega - E_{\mathrm{g0}}\right)^m$, where m is a numeric constant governed by the prevailing *direct interband* (*allowed* and *forbidden*) transitions taking place in the semiconductor (Tauc, 1972; Tauc, 1979; Heavens, 1991; Azzam & Bashara, 1987; Ward, 1994; Dragoman & Dragoman, 2002; Stenzel, 2005; Forouhi & Bloomer, 1986; Forouhi & Bloomer, 1988; Adachi, 1991; Jellison & Modine, 1996; Chambouleyron & Martínez, 2001; Truong & Tanemura, 2006; Kasap & Capper, 2006; Christman, 1988; Rogalski & Palmer, 2000; Palik, 1998; Dressel & Grüner, 2002; Dresselhaus, 2001; Bassani & Parravicini, 1975; Sólyom, 2009). The frequency dependency of $\epsilon''(\omega)$ or $\alpha(\omega)$ of a crystalline semiconductor due to *direct interband* transitions is often written in a closed analytical form that is applicable in a narrow range of photon energies around absorption edge as

$$\epsilon''_{\mathrm{dir}}(\omega) \equiv \left(\frac{c\, n(\omega)\, \alpha_{\mathrm{dir}}(\omega)}{\omega}\right) = \begin{cases} 0, & \hbar\omega < E_{\mathrm{g0}} \\ D_\epsilon \frac{\left(\hbar\omega - E_{\mathrm{g0}}\right)^m}{(\hbar\omega)^2}, & \hbar\omega \geq E_{\mathrm{g0}} \end{cases} \tag{14}$$

where D_ϵ is a frequency- and temperature- independent parameter governed by type and band structure of the material and m is $1/2$ and $3/2$ for *allowed* and *forbidden direct interband* electronic transitions, respectively (Tauc, 1972; Tauc, 1979; Heavens, 1991; Azzam & Bashara, 1987; Ward, 1994; Dragoman & Dragoman, 2002; Stenzel, 2005; Forouhi & Bloomer, 1986; Forouhi & Bloomer, 1988; Adachi, 1991; Jellison & Modine, 1996; Chambouleyron & Martínez, 2001; Truong & Tanemura, 2006; Kasap & Capper, 2006; Christman, 1988; Rogalski & Palmer, 2000; Palik, 1998; Dressel & Grüner, 2002; Dresselhaus, 2001; Bassani & Parravicini, 1975; Sólyom, 2009). The respective $\epsilon'_{\mathrm{dir}}(\omega)$-function that is limited to spectral range in the vicinity of absorption edge (interband region), where $\epsilon''_{\mathrm{dir}}(\omega)$-formula of Equation (14) is valid, can be found from the $\epsilon'(\omega)$-Kramers-Kronig-relation (KKR), which ought to be evaluated over a very wide spectral range from 0 to *infinity* and not for the interband spectral region; however, such a difficulty can be overcome by multiplying the $\epsilon''_{\mathrm{dir}}(\omega)$-Equation (14) by a *step function* of the *Heaviside type*: $\Theta(1-z) \equiv 1$ for $z \leq 1$ and $\Theta(1-z) \equiv 0$ for $z > 1$, with $z = E_{\mathrm{g0}}/\hbar\omega$ (Theiss, 2012; Adachi, 1991). When the measured absorption coefficient $\alpha(\omega)$ of a *direct* bandgap crystalline substance is properly plotted as a function of the photon energy $\hbar\omega$, in accordance with the functional form given in Equation (14) for $m = 1/2$ (allowed direct interband transitions)

or $m = 3/2$ (forbidden direct interband transitions), we obtain a linear-like portion, usually in a limited frequency range. The extrapolation of the obtained linear part to zero absorption coefficient (i.e., the crossing point with the $\hbar\omega$-axis) yields a threshold frequency ω_{g0} corresponding to its fundamental absorption edge- that is, $E_{\mathrm{g0}} = \hbar\omega_{\mathrm{g0}}$, which is, of course, a slightly decreasing function with the ambient sample temperature T, the maximum value of which is at absolute zero ($T = 0\mathrm{K}$).

In a crystalline *indirect-band* semiconductor, both direct and indirect interband transitions take place upon illuminating it by light of apt angular frequency ω and wavevector $\mathbf{k}_{ph}$. The indirect interband transitions occur between initial valence-band states $\mathrm{v}\mathbf{k}_i$ and final conduction-band states $\mathrm{c}\mathbf{k}_f$ ($\neq \mathrm{v}\mathbf{k}_i$) and separated in energy by $E_{\mathrm{c}}(\mathrm{c}\mathbf{k}_f) - E_{\mathrm{v}}(\mathrm{v}\mathbf{k}_i)$ via the participation of phonons of normal-mode lattice-vibration spectra of the solid (Tauc, 1972; Tauc, 1979; Heavens, 1991; Azzam & Bashara, 1987; Ward, 1994; Dragoman & Dragoman, 2002; Stenzel, 2005; Forouhi & Bloomer, 1986; Forouhi & Bloomer, 1988; Adachi, 1991; Jellison & Modine, 1996; Chambouleyron & Martínez, 2001; Truong & Tanemura, 2006; Kasap & Capper, 2006; Christman, 1988; Rogalski & Palmer, 2000; Palik, 1998; Dressel & Grüner, 2002; Dresselhaus, 2001; Bassani & Parravicini, 1975; Sólyom, 2009). Each phonon has an energy $E_{\mathrm{phon}} = \mathrm{k_B}\theta = \hbar\omega_{\mathbf{q}_0}$ and wavevector $\mathbf{q}_0$, which connect the various valence and conduction bands extrema states having $\mathrm{c}\mathbf{k}_f$ and $\mathrm{v}\mathbf{k}_i$ in the first Brillouin zone, where $\mathrm{k_B}$ is the Boltzmann constant and θ is a lattice temperature. For an indirect-bandgap crystalline semiconductor, the lowest energy between uppermost $\mathrm{v}\mathbf{k}_i$-energy states in valence band and allowed $\mathrm{c}\mathbf{k}_f$-energy states in conduction band is its *indirect* bandgap energy $E_{\mathrm{g}}^{\mathrm{ind}} = E_{\mathrm{c}}(\mathrm{c}\mathbf{k}_f) - E_{\mathrm{v}}(\mathrm{v}\mathbf{k}_i)$, which is less than E_{g0}. Optical absorption due to photon-electron-phonon interactions in an indirect-bandgap crystal is only feasible if the total energy and momenta conservation rules $\hbar\omega - E_{\mathrm{g}}^{\mathrm{ind}} \pm \hbar\omega_{\mathbf{q}_0} = 0$ and $\mathbf{k}_{ph} + \mathrm{v}\mathbf{k}_i \pm \mathbf{q}_0 = \mathrm{c}\mathbf{k}_f$ are both fulfilled, with the $\pm$ sign indicates that for electrons in valence band to get to energy states in conduction band of unlike wavevectors, indirect interband transitions occur by absorption ($+$) or emission ($-$) of phonons when the crystal is illuminated with photons of energy $\hbar\omega < E_{\mathrm{g}}^{\mathrm{ind}}$ or $E_{\mathrm{g0}} > \hbar\omega \geq E_{\mathrm{g}}^{\mathrm{ind}}$, respectively. For small photon energies such that $\hbar\omega < E_{\mathrm{g}}^{\mathrm{ind}} = E_{\mathrm{c,min}}(\mathrm{c}\mathbf{k}_f) - E_{\mathrm{v,max}}(\mathrm{v}\mathbf{k}_i)$, no indirect interband transitions would occur in a perfectly crystalline indirect-gap semiconductor, but for high photon energies such that $\hbar\omega \geq E_{\mathrm{g0}}$, the probability for the direct interband electronic transitions to take place is much higher than that corresponds to indirect interband transitions, which would occur for photon energies satisfying the condition $E_{\mathrm{g0}} > \hbar\omega \geq E_{\mathrm{g}}^{\mathrm{ind}}$. Indirect interband transitions have strong dependence on the sample's ambient temperature via the Boltzmann energy term $e^{E/\mathrm{k_B}T}$ in the Planck's or statistical Bose-Einstein distribution law that determines the average occupation number n_q of phonons (bosons in general) of energy E at the absolute temperature T, which is given by $n_q(\omega_{\mathbf{q}_0}, T) \equiv \{\exp(\hbar\omega_{\mathbf{q}_0}/\mathrm{k_B}T) - 1\}$ (Christman, 1988; Rogalski & Palmer, 2000; Palik, 1998; Dressel & Grüner, 2002; Reitz et al., 1993; Bassani & Parravicini, 1975). The contribution of *direct interband transitions* to the dielectric function and absorption of an indirect-bandgap of a crystalline, defect-free sample can be determined from Equation (14), which usually display rather weak temperature dependency, mostly as a result of the slight variation of the bandgap energy of the substance with its ambient temperature. The contributions $\alpha_{+}^{\mathrm{ind}}(\omega)$ and $\alpha_{-}^{\mathrm{ind}}(\omega)$ of the *one-photon phonon-assisted indirect interband* transitions via absorption ($+$) and emission ($-$) of phonons in a perfect crystal to its total absorption coefficient $\alpha_{\mathrm{tot}}^{\mathrm{ind}}(\omega)$ can be, assuming parabolic energy bands and approximately-constant transition matrix elements (i.e., independent of $\mathrm{c}\mathbf{k}_i$ and $\mathrm{c}\mathbf{k}_f$), written in the form (Bassani & Parravicini, 1975)

$$\alpha_{\mathrm{tot}}^{\mathrm{ind}} = \alpha_{+}^{\mathrm{ind}}(\omega) + \alpha_{-}^{\mathrm{ind}}(\omega) = \frac{B}{\hbar\omega\, n(\omega)}\left\{\frac{\left(\hbar\omega - E_{\mathrm{g}}^{\mathrm{ind}} + E_{\mathrm{phon}}\right)^2}{\left[e^{+(\hbar\omega_{\mathbf{q}_0}/\mathrm{k_B}T)} - 1\right]} + \frac{\left(\hbar\omega - E_{\mathrm{g}}^{\mathrm{ind}} - E_{\mathrm{phon}}\right)^2}{\left[1 - e^{-(\hbar\omega_{\mathbf{q}_0}/\mathrm{k_B}T)}\right]}\right\} \tag{15}$$

The pre-factor B is regarded to be independent of wavevectors $\mathrm{c}\mathbf{k}_i$ and $\mathrm{c}\mathbf{k}_f$ in conduction and valence bands and is a constant of the material. The total absorption coefficient $\alpha_{\mathrm{tot}}^{\mathrm{ind}}(\omega)$ due to *allowed indirect* interband transitions in a crystal depends quadratically on the photon energy $\hbar\omega$ and, for a given $\mathbf{q}_0$, both absorbed and emitted phonons participate in optical transitions. For phonon-assisted indirect interband transitions, the plot of $\sqrt{\hbar\omega\,\alpha(\omega)}$-versus-$\hbar\omega$ at a given temperature T may display low- and high- frequency linear portions, the intersections of which with the $\hbar\omega$-axis correspond to two threshold frequencies $\hbar\omega_{\mp} = E_{\mathrm{g}}^{\mathrm{ind}} \mp E_{\mathrm{phon}}$ involving absorption ($-$) and emission ($+$) of phonons with the energy $\hbar\omega_{\mathbf{q}_0}$, from which the phonon frequency $\omega_{\mathbf{q}_0} = (\omega_{+} - \omega_{-})/2$ and absorption edge frequency $\omega_{\mathrm{g}}^{\mathrm{ind}} = (\omega_{-} + \omega_{+})/2$ can be determined. At low temperatures, there are no phonons to be absorbed and only the contribution of $\alpha_{-}^{\mathrm{ind}}(\omega)$ due to phonon emission is important, but as T increases, the contribution of $\alpha_{+}^{\mathrm{ind}}(\omega)$ comes in with the relative intensity governed by the Boltzmann factors $e^{\pm(\hbar\omega_{\mathbf{q}_0}/\mathrm{k_B}T)}$. Forbidden *indirect* interband transitions are also possible, with an analytical functional form for the absorption coefficient on photon energy $\hbar\omega$ and sample's ambient temperature T being analogous to that of *allowed indirect* interband transitions, but with a smaller transition

probability and power-law dependency on $\hbar\omega$ as $\alpha^{\text{ind}}_{\pm\,\text{forbid}}(\omega) \propto \left(\hbar\omega - E^{\text{ind}}_{\text{g}} \pm E_{\text{phon}}\right)^3 / [\hbar\omega\, n(\omega)]$ (Ward, 1994; Dragoman & Dragoman, 2002; Stenzel, 2005).

2.3.2.2 Interband and Sub-Bandgap Dielectric Functions for Undoped Amorphous Semiconductors

There are few reported formulations that describe dispersion and absorption phenomena in structurally disordered amorphous semiconductors in the interband transition region (Innami et al., 1999; Tauc, 1972; Tauc, 1979; Forouhi & Bloomer, 1988; Adachi, 1991; Jellison & Modine, 1996), but the frequency dependence of their complex dielectric constant $\hat{\epsilon}(\omega) \equiv \epsilon'(\omega) + j\epsilon''(\omega)$ in both interband transition and sub-bandgap regions are still subjected to controversy. It is of both technological importance and scientific interest to have closed-form analytical expressions of $\hat{\epsilon}(\omega)$ to describe as-measured optical response of amorphous semiconductors and reveal their energy band structures. This is motivated by the fact that valence and conduction bands retain their meaning in amorphous materials and that conservation of energy of the photon-electron system is still satisfied in the course of band-to-band optical transitions, though momentum (wavevector $\mathbf{k}$) is a poor quantum number. Assuming that the basic volume V contains the same number of atoms in the amorphous as in crystalline sates and the momentum transition matrix element $\mathbf{M}_{\text{cv}}(\mathbf{k})$ is independent of wavevector $\mathbf{k}$, Tauc (Tauc, 1972; Tauc, 1979) described the imaginary part $\epsilon''(\omega)$ of the complex dielectric constant of an amorphous semiconductor by the quantum-mechanical $\epsilon''(\omega)$-formula of a perfect crystal given in Equation (9) with Equation (13) for the joint-density-of-states $\mathcal{J}_{\text{cv}}(\hbar\omega)$ of occupied valence-band and empty conduction-band states involved in interband transitions separated in energy by $\hbar\omega$, as is typified by the expression

$$\epsilon''(\omega) = \frac{e^2}{\epsilon_0 m_e^{*2}\omega^2} |\hat{\boldsymbol{e}}.\mathbf{M}_{\text{cv}}(\mathbf{k})|^2 \int_{-\infty}^{\infty} \text{g}_{\text{c}}(E^*)\, \text{g}_{\text{v}}(\hbar\omega - E^*) dE^* \tag{16}$$

In amorphous undoped semiconductors, $\text{g}_{\text{c}}(E)$ and $\text{g}_{\text{v}}(E)$ still represent, respectively, the densities of states (DOS) per unit volume in conduction and valence bands, however, they had to be modified, compared to those of crystalline undoped semiconductors, to take into account localized energy states lying in the bandgap of the substance. Consider a disorderless, defect-free, and undoped semiconductor or dielectric with simple isotropic and parabolic valence and conduction bands, at least in a certain range of wavevectors about their extremes, and with the edges of its conduction and valence bands are located, relative to a zero-energy reference, at the energies E_{c} and E_{v}, respectively. The dependency of its conduction-band DOS $\text{g}_{\text{c}}(E)$ and valence-band DOS $\text{g}_{\text{v}}(E)$ on the energy E, where $\text{g}_{\text{c}}(E)$ and $\text{g}_{\text{v}}(E)$ are supposed to terminate abruptly at the band edges E_{c} and E_{v}, can be shown to have the parabolic-like analytical functional form given below (Christman, 1988; Rogalski & Palmer, 2000; Palik, 1998; Dressel & Grüner, 2002; Reitz et al., 1993)

$$\text{g}_{\text{c}}(E) = \frac{\sqrt{2} m_{\text{c}}^{*3/2}}{\pi^2\hbar^3} \begin{cases} \sqrt{E - E_{\text{c}}}, & E \geq E_{\text{c}} \\ 0, & E < E_{\text{c}} \end{cases} \tag{17}$$

$$\text{g}_{\text{v}}(E) = \frac{\sqrt{2} m_{\text{v}}^{*3/2}}{\pi^2\hbar^3} \begin{cases} 0, & E > E_{\text{v}} \\ \sqrt{E_{\text{v}} - E}, & E \leq E_{\text{v}} \end{cases} \tag{18}$$

where m_{c}^* and m_{v}^* are the DOS's effective masses associated with the conduction and valence bands of the solid or the so-called conduction-band and valence-band density-of-states effective masses, respectively, which are determined by their respective band structures in the different directions of wavevectors (Christman, 1988; Rogalski & Palmer, 2000; Palik, 1998; Dressel & Grüner, 2002; Reitz et al., 1993). Assuming parabolic and isotropic conduction and valence bands of the forms given in Equations (17) and (18) and the radiation-field-induced electronic (optical) transitions taking place between the occupied valence-band and empty (available) conduction-band energy states separated by an energy $\hbar\omega$, Tauc (Tauc, 1972; Tauc, 1979) obtained a closed analytical form for the variation of $\epsilon''(\omega)$ of a disordered non-crystalline (amorphous) semiconductor with the exciting photon energy $\hbar\omega$ given by the expression

$$\epsilon''_T(\omega) = A_T \frac{\left(\hbar\omega - E_{\text{g}}^{\text{opt}}\right)^2}{(\hbar\omega)^2} \tag{19}$$

where A_T is a non-dimensional parameter characteristics of the material and $E_{\text{g}}^{\text{opt}}$ is the so-called optical (Tauc) bandgap energy. The $\epsilon''_T(\omega)$-model is to some extent analogous to the absorption model describing *allowed indirect interband* optical transitions in *crystalline* semiconductors of the form given by Equation (15), with the conservation of the energy of the photon-electron system but not of its momentum being significant. Equation (19) is only applicable for describing interband transition mechanisms (optical absorption) in a limited range of exciting photon energies in the neighborhood of the material absorption edge with $\epsilon''_T(\omega) = 0$ for $\hbar\omega < E_{\text{g}}^{\text{opt}}$

and $\epsilon_T''(\omega) > 0$ for $\hbar\omega \geq E_g^{opt}$; of course, however, defect-related, sub-bandgap, and intraband optical absorptions may exist in a real amorphous semiconductor which will render its $\epsilon''(\omega) > 0$ for $\hbar\omega < E_g^{opt}$, but such effects are not explicitly included in the Tauc dielectric model. The experimentally observed optical spectra of absorption coefficient $\alpha(\omega)$, or extinction coefficient $\kappa(\omega)$, or imaginary part $\epsilon''(\omega)$ of the complex dielectric constant of linear, isotropic, non-magnetic, and undoped amorphous semiconductors, which are inter-connected through the relationship $\alpha(\omega) \equiv \omega\epsilon''(\omega)/c\, n(\omega) \equiv 2\,\omega\kappa(\omega)/c$, can be hypothetically divided into two major spectral regimes. One regime is allocated to the high-absorption region where $\alpha(\omega) > \alpha_c$, where α_c is a cross-over numerical value in the approximate range of $10^3 - 10^4 \text{cm}^{-1}$, depending on the material. In such high-absorption region, the Tauc $\epsilon_T''(\omega)$-relation and a variety of different variations of it that were commonly adopted to describe $\epsilon''(\omega)$ of an amorphous substance or its $\kappa(\omega)$, assuming $n(\omega)$ is constant in the interband transition region have form

$$\epsilon''(\omega) = A_\epsilon \frac{\left(\hbar\omega - E_g^{opt}\right)^m}{(\hbar\omega)^2} \qquad \text{or} \qquad \kappa(\omega) \cong A_\kappa \frac{\left(\hbar\omega - E_g^{opt}\right)^m}{(\hbar\omega)^2} \tag{20}$$

For most pure non-crystalline dielectric and undoped amorphous semiconductors, including undoped amorphous selenium (*a*-Se), the commonly reported literature values of the exponent parameter m were 2 and 3; however, it has been argued that the power-law frequency dependence of $\epsilon''(\omega)$ and $\kappa(\omega)$ described in Equation (20) is approximately valid for undoped *a*-Se as well, but with $m \cong 1$ (Mott & Davis, 1979). The other spectral absorption regime is habitually assigned to the structural-disorder and defect-related low-absorption region below the absorption edge of amorphous (non-crystalline) dielectrics and semiconductors where $\alpha(\omega) < \alpha_c$, with the extinction coefficient $\kappa(\omega)$ is always debated to exhibit a linear-exponential dependence on the exciting photon energy $\hbar\omega$ and on the sample's ambient temperature T, the so-called Urbach-tail behavior, of the analytical form given by (Mott & Davis, 1979; Nagels et al., 1995; Tichy et al., 1996; Nagels et al., 1997)

$$\kappa(\hbar\omega, T) \equiv c\,\alpha(\hbar\omega)/2\omega = A_\kappa \exp\left[(\hbar\omega - E_0)/\Gamma_U(T)\right]/\hbar\omega \tag{21}$$

The parameters A_ϵ and A_κ are different constants of the amorphous material, E_0 is an energy constant comparable to E_g^{opt}, and $\Gamma_U(T)$ is a temperature-dependent energy parameter that signifies the extent of energy states below absorption edge, referred to as the breadth of absorption (Urbach-) tail, neither its origin nor temperature dependency is a definitely solved problem, with a variety of formulations for its variation with temperature (Nagels et al., 1995; Tichy et al., 1996; Nagels et al., 1997). To limit the Tauc $\epsilon''(\omega)$-model to the interband spectral region of an amorphous semiconductor and to make mathematical evaluation of the respective real part $\epsilon'(\omega)$ of its complex dielectric constant feasible and physically meaningful, a phenomenological broadening term $j\Gamma$ has been added to the photon energy $\hbar\omega$, in addition to multiplying the $\epsilon''(\omega)$-formulation given in Equation (19) by step functions of the Heaviside type to account for cutoff energies at the absorption edge and high-energy side (Adachi, 1991).

2.3.3 The Jellison-Modine (Tauc-Lorentz) Interband Dielectric Mode for Amorphous Materials

To overcome some of the practicability limitations in the Forouhi and Bloomer (FB) optical dispersion functions, in addition to account for the band-to-band optical absorption in an undoped amorphous semiconductor or insulator, Jellison and Modine (Jellison & Modine, 1996) proposed an empirical model for the frequency dependence of its dielectric function $\epsilon''(\omega)$ via multiplying the Tauc joint-density-of states $\epsilon_T''(E)$-model given in Equation (19), where $E = \hbar\omega$, the exciting photon energy, by the $\epsilon_L''(E)$-Lorentz harmonic dispersion model for a collection of non-interacting atoms. The $\epsilon_L''(E)$-formulation can be accomplished either from standard quantum-mechanical treatment of the Hamiltonian of microscopic electric dipoles in the presence of electromagnetic radiation or, equivalently, from a Lorentz harmonic oscillator approach, which can be written in terms of an energy-like amplitude A_L, a peak transition energy E_0 $(= \hbar\omega_0$, where ω_0 is a resonance frequency), a broadening (damping) energy term C $(= \hbar\omega_\tau$, where ω_τ is a damping frequency) as expressed below (Innami et al., 1999; Jellison & Modine, 1996)

$$\epsilon_L''(E) = 2n(E)\kappa(E) = \frac{A_L C E_0 E}{\left(E^2 - E_0^2\right)^2 + C^2 E^2} \tag{22}$$

In the Jellison-Modine model, the so-called Tauc-Lorentz $\epsilon_{TL}''(E)$-dielectric model, parameterization of the optical constants $n(E)$ and $\kappa(E)$ of amorphous tetrahedral semiconductors can be addressed, for a single-oscillator term, by making use of their combined $\epsilon_{TL}''(E)$-formulation given in the form (Innami et al., 1999; Jellison & Modine, 1996)

$$\epsilon''_{TL}(E) = \begin{cases} \frac{1}{E} \frac{A_L C E_0 A_T \left(E - E_g^{opt}\right)^2}{\left(E^2 - E_0^2\right)^2 + C^2 E^2}, & E > E_g^{opt} \\ 0, & E \leq E_g^{opt} \end{cases} \quad (23)$$

The formulation of the real part $\epsilon'_{TL}(E)$ of the complex dielectric constant of amorphous semiconductors and insulators corresponding to the Tauc-Lorentz $\epsilon''_{TL}(E)$-formula can be obtained by making use of the Kramers-Kronig (KK) transformation $\epsilon'(E)$-integral described by the general expression (Jellison & Modine, 1996)

$$\epsilon'_{TL}(E) = \epsilon'(\infty) + \frac{2}{\pi} P \int_{E_g^{opt}}^{\infty} \frac{\xi \epsilon''_{TL}(\xi)}{(\xi^2 - E^2)} d\xi \quad (24)$$

The symbol P stands for the Cauchy principal part of the integral and $\epsilon'(\infty)$ is introduced, instead of unity in the KK ϵ'-relation, as an adjustable fitting parameter to account for a high-frequency contribution to dielectric constant. The closed form analytical $\epsilon'_{TL}(E)$-formula is, however, quite unwieldy (Innami et al., 1999; Jellison & Modine, 1996), and no need to cite here. The absorption given by Equation (23) corresponds to interband transitions and manifests itself as a rapid rise in optical absorption obeying the Tauc power–law $\left(E - E_g^{opt}\right)^2 / E^2$, while the Lorentz term $E/[(E^2 - E_0^2)^2 + C^2 E^2]$ provides the decrease in optical absorption at high photon energies. The conditions put on E in Equation (23) to make $\epsilon''_{TL}(E) = 0$ for $E \leq E_g^{opt}$ and to get a Tauc-Lorentz $\epsilon''_{TL}(E)$-formula with interband optical absorptions at photon energies larger than E_g^{opt}, the $\epsilon''_{TL}(E)$-formula is multiplied by a Heaviside function $\Theta\left(E - E_g^{opt}\right)$ (Theiss, 2012; Adachi, 1991). For a semiconductor, the $\epsilon''_{TL}(E)$-spectrum of Tauc-Lorentz (TL) model shows a single broad-peak structure with a maximum in nearby $E \sim E_0$, the transition energy, which is expected in amorphous tetrahedral semiconductors. The Tauc-Lorentz $\epsilon''_{TL}(E)$-model implies that optical absorptions in an amorphous sample due to defects, intraband processes, or Urbach-tail localized energy states in bandgap arising from disorder broadening of undistorted energy bands will increase $\epsilon''_{TL}(E)$ and render it non-zero at sub-bandgap photon energies- that is, $\epsilon''_{TL}(E) > 0$ for $E < E_g^{opt}$. The $\epsilon''_{TL}(E)$- and/or $\epsilon'_{TL}(E)$- relations contain four unknowns to be dogged and cannot be used to calculate them directly at each E from values of $\epsilon''_{TL}(E)$ or $\epsilon'_{TL}(E)$; yet, the common approach to extract them is to curve fit such formulas to as-measured $\epsilon''_{TL}(E)$- and $\epsilon'_{TL}(E)$- E data in a spectral range. If electronic transitions occur between energy states in various valence and conduction bands, as in *a*-Se whose band structure composed of five local conduction and valence bands (Innami et al., 1999), the Jellison-Modine (JM) model (Jellison & Modine, 1996) had to be modified to include all band-to-band transitions. For *a*-Se, the JM model was extended by Innami et al. (1999) to a combination of *four* analogous TL $\epsilon''_{TL,i}(E)$- and $\epsilon'_{TL,i}(E)$- formulas, with each has its own four parameters and exhibit a broad peak on its $\epsilon''_{TL,i}(E)$ spectrum around E_{0i} $(i = 1 - 4)$, which they used to discuss ellipsometric absorption spectra of their *a*-Se films, evaporated on Si (100) substrates from starting Se-ingots of purity 99.9999%. Their $\epsilon''_{TL}(E)$-spectra exhibit a collective effect of four band contributions, prevailing in diverse spectral ranges, but their curve-fitting program incorporated 16 unlike fit parameters.

2.3.4 The O'Leary-Johnson-Lim (OJL) Interband Transition Dielectric Model

First, note that Innami et al. (1999) found no significant surface microroughness overlayer on top of their selenium films, while others (Nagels et al., 1997) reported a substantial roughness layer for their thermally evaporated *a*-Se films on glass substates of similar film thicknesses. Also, few workers (Tan, 2006; Tan et al., 2007; Tan et al., 2006; Solieman & Abu-Sehly, 2010; Nagels et al., 1995; Tichy et al., 1996) considered structural disorder of their *a*-Se films and existence of native defects, which give rise to Urbach tails of localized energy states in the *a*-Se bandgap. The analysis of optical absorption and dispersion spectra of a semiconductor by the interband Tauc-dielectric model and sub-bandgap Urbach model are based on the fact that its dielectric constants are directly given, as in ellipsometry, which are less sensitive for absorption coefficients less than 10^3cm^{-1} and the directly measured quantities are sensitive to miniature bulk and surface structural features of the sample. The dielectric and optical constants cannot, however, at all times be extracted from as-measured specular transmittance and/or reflectance spectra of multi-layered film structures the sample investigated, as their respective theoretical formulations are much involved and intricate in particular when multiple internal light-wave reflections inside the films (layers) of such optical systems and the effects of interference between them are significant.

A modeling approach that can be employed to extract the dielectric and optical parameters of disordered amorphous semiconducting films deposited onto substrates of unlike optical properties from their experimental transmittance and/or reflectance spectra and that incorporates interband and sub-bandgap dielectric models is appealing. From a practical point of view, the presence of a significant amount of structural disorder, native

impurities, defects and imperfections in amorphous semiconducting films renders their energy band structures to be complicated and are not properly defined compared to those band structures of disorderless sample made from the same material. Yet, the valence and conduction bands of disordered samples retain their meaning and manifested themselves in their density of energy states functions involved in the formulations describing their dielectric and optical properties that should be modified to account for effects due to native impurities, structural disordering, and amorphousity in non-crystalline substances.

An approach to model the influence of structural disorder of an undoped amorphous semiconductor on its optical spectra is to assume that the DOS functions of parabolic valence and conduction bands do not terminate abruptly at their edges, but smeared out and extend into bandgap to form band tails of localized energy states above and below band edges. The actual functional form of the DOS in band tails is somewhat difficult to specify adequately and is still controversial, but the transition in DOS function between the band region and tail region is a smooth one (O'Leary et al., 1997; Dias da Silva et al., 2004); however, from both experimental and theoretical points of view, we can assume a distribution of localized states in such band tails that can be approximately represented by smooth linear-exponential-like functional dependency on E, as was proposed by O'Leary and his co-workers (O'Leary et al., 1997; Dias da Silva et al., 2004). The square-root-power-law functional energy dependencies of the DOS $\mathrm{g_c}(E)$ and $\mathrm{g_v}(E)$ given in Equations (17) and (18), which are associated with well-defined and sharped-edge parabolic valence and conduction energy bands, can be modified to have closed analytical forms described by the expressions (O'Leary et al., 1997; Dias da Silva et al., 2004)

$$\mathrm{g_c}(E) = \frac{\sqrt{2}m_{\mathrm{c}}^{*3/2}}{\pi^2\hbar^3}\begin{cases}\sqrt{E-E_{\mathrm{c}}}, & E \geq E_{\mathrm{c}} + \frac{\gamma_{\mathrm{c}}}{2} \\ \sqrt{\frac{\gamma_{\mathrm{c}}}{2}}\exp\left(-\frac{1}{2}\right)\exp\left(\frac{E-E_{\mathrm{c}}}{\gamma_{\mathrm{c}}}\right), & E < E_{\mathrm{c}} + \frac{\gamma_{\mathrm{c}}}{2}\end{cases} \tag{25}$$

$$\mathrm{g_v}(E) = \frac{\sqrt{2}m_{\mathrm{v}}^{*3/2}}{\pi^2\hbar^3}\begin{cases}\sqrt{\frac{\gamma_{\mathrm{v}}}{2}}\exp\left(-\frac{1}{2}\right)\exp\left(\frac{E_{\mathrm{v}}-E}{\gamma_{\mathrm{v}}}\right), & E \geq E_{\mathrm{v}} - \frac{\gamma_{\mathrm{v}}}{2} \\ \sqrt{E_{\mathrm{v}}-E}, & E < E_{\mathrm{v}} - \frac{\gamma_{\mathrm{v}}}{2}\end{cases} \tag{26}$$

The energies E_{c} and E_{v} denote, respectively, the sharp edges of conduction and valence bands in the absence of structural disorder, while γ_{c} and γ_{v} are the broadening spreads of their respective tails into the semiconductor's bandgap that increase with increasing in its structural disorder. The energy terms $E_{\mathrm{c}} + \gamma_{\mathrm{c}}/2$ and $E_{\mathrm{v}} - \gamma_{\mathrm{v}}/2$ signify the transition points between the square-root and linear-exponential distribution of energy states within the bands and into the bandgap region, with their DOS functions $\mathrm{g_c}(E)$ and $\mathrm{g_v}(E)$, with their first derivatives being continuous at these points (Benkhedir, 2006; Theiss, 2012; O'Leary et al., 1997; Dias da Silva et al., 2004). Let all band-tail energy states to be localized and all band energy states to be extended, the energy levels $E_{\mathrm{c}}^{\mathrm{mob}} = E_{\mathrm{c}} + \gamma_{\mathrm{c}}/2$ and $E_{\mathrm{v}}^{\mathrm{mob}} = E_{\mathrm{v}} - \gamma_{\mathrm{v}}/2$ represent the so-called *mobility edges* of the conduction and valence bands, respectively, with the energy difference $E_{\mathrm{g}}^{\mathrm{mob}} = E_{\mathrm{c}}^{\mathrm{mob}} - E_{\mathrm{v}}^{\mathrm{mob}} = E_{\mathrm{g0}} + (\gamma_{\mathrm{c}} + \gamma_{\mathrm{v}})/2$ is the *mobility-edge bandgap energy*, where $E_{\mathrm{g0}} = (E_{\mathrm{c}} - E_{\mathrm{v}})$ is the Tauc absorption edge or Tauc bandgap energy in the disorderless limit- that is, when $\gamma_{\mathrm{c}} \to 0$ and $\gamma_{\mathrm{v}} \to 0$. Such DOS features that accompany the parabolic-like conduction and valence energy bands of an undoped amorphous semiconductor with a significant amount of structural disorder and imperfection is schematically illustrated in Figure (1).

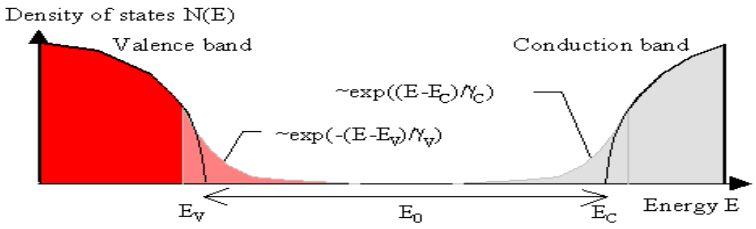

Figure 1. Schematic diagram of the density-of-states DOS in parabolic valence and conduction energy bands and their linear-exponential energy distribution tail states for an undoped disordered semiconductor (Benkhedir, 2006; Theiss, 2012)

Optical absorptions in disordered amorphous semiconductor with tails of localized energy states in its bandgap can result from four types of radiation-induced electronic transitions as depicted in Figure (2). Transitions can occur

between occupied valence-band extended states below mobility edge $E_{\mathrm{v}}^{\mathrm{mob}}$ ($=E_{\mathrm{v}}-\gamma_{\mathrm{v}}/2$) and empty conduction-band extended states above mobility edge $E_{\mathrm{c}}^{\mathrm{mob}}$ ($=E_{\mathrm{c}}+\gamma_{\mathrm{c}}/2$), and this needs photon energies larger than $E_{\mathrm{g}}^{\mathrm{mob}}$, which is larger than the disorderless bandgap energy E_{g0} by the amount $(\gamma_{\mathrm{c}}+\gamma_{\mathrm{v}})/2$. Optical absorptions may also related to transitions between occupied valence-band extended states below $E_{\mathrm{v}}^{\mathrm{mob}}$ and empty conduction-band localized states tail below $E_{\mathrm{c}}^{\mathrm{mob}}$ or, equally with the same momentum matrix element strength, from electronic transitions between occupied localized states in valence-band tail and empty extended states in conduction band. In a disordered semiconductor, an optical transition would occur among occupied localized states in valence-band tail and empty localized states in conduction-band tail.

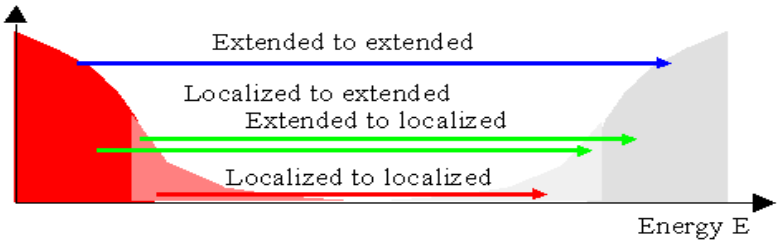

Figure 2. Optical absorptions in a disordered amorphous semiconductor via electronic transitions among extended states in valence band and localized states in its tail and extended states in conduction band and localized states in its tail

The radiation-induced electronic transitions in an undoped amorphous semiconductor with structural disorder manifest themselves in the dependency of its absorption coefficient $\alpha(\hbar\omega)\equiv\{\omega\,\epsilon''(\hbar\omega)/c\,n(\hbar\omega)\}$ on $\hbar\omega$, which can be verbalized in terms of the joint-density-of-states (JDOS) function $\mathcal{J}_{\mathrm{cv}}(\hbar\omega)$ associated with its broadened conduction and valence bands and optical transition matrix element $D^2(\hbar\omega)$ by the following general expression (O'Leary et al., 1997; Dias da Silva et al., 2004)

$$\alpha(\hbar\omega)=D^2(\hbar\omega)\,\mathcal{J}_{\mathrm{cv}}(\hbar\omega)=D^2(\hbar\omega)\int_{-\infty}^{\infty}\mathrm{g_c}(E^*)\,\mathrm{g_v}(\hbar\omega-E^*)dE^* \tag{27}$$

For an undoped amorphous semiconductor with structural disorder, the energy dependency of conduction- and valence- band DOS $\mathrm{g_c}(E^*)$ and $\mathrm{g_v}(E^*)$ is given in Equations (25) and (26) with $\gamma_{\mathrm{c}}\neq\gamma_{\mathrm{v}}\neq 0$, which reduce to the simple parabolic forms of Equations (17) and (18) in the disorderless limit, i.e., $\gamma_{\mathrm{c}}\to 0$ and $\gamma_{\mathrm{v}}\to 0$. The exact functional dependence of $D^2(\hbar\omega)$ on photon energy remains uncertain yet, though it was reported that $D^2(\hbar\omega)$ exhibits smooth variation with ω in case of optical absorptions from extended-state-to-extended-state, extended-state-to-localized-state, and localized-state-to-extended-state electronic transitions, and if the momentum matrix element is constant, $D^2(\hbar\omega)\propto 1/\hbar\omega$ (O'Leary et al., 1997). Optical absorptions in a disordered semiconductor due to extended-state-to-extended-state transitions obey Tauc-like $\epsilon''_{TL}(E)$-model, with a mobility-edge gap energy $E_{\mathrm{g}}^{\mathrm{mob}}$ ($>E_{\mathrm{g0}}$), while optical absorptions occurring via extended-state-to-localized-state and localized-state-to-extended-state radiation-induced transitions are described by the temperature-dependent Urbach $\alpha(\hbar\omega,T)$ -relation (21), with the energy parameter $E_0\sim E_{\mathrm{g0}}$. Localized-state-to-localized-state optical transitions in disordered semiconductors are less significant, compared with other transitions, because there are a limited number of localized energy states in the tails of conduction and valence bands and their optical transition matrix element $D^2(\hbar\omega)$ is much smaller, and this kind of optical transitions is effective for low photon energies in the infrared. Based on the DOS functions of Equations (25) and (26) for parabolic valence and conduction bands of an amorphous semiconductor with linear-exponential distribution of localized states in their tails encroaching bandgap, a closed form functional frequency dependency of its absorption coefficient $\alpha(\hbar\omega)$ was skilled by O'Leary, Johnson and Lim (OJL) (O'Leary et al., 1997). They showed that $\alpha(\hbar\omega)$ of a disordered amorphous semiconductor is given in terms of an optical transition matrix element $D^2(\hbar\omega)\propto 1/\hbar\omega$ multiplied by a set of intricate analytical expressions for the joint-density-of-states (JDOS) $\mathcal{J}_{\mathrm{OJL}}(\hbar\omega)$ function that combine energy states in conduction and valence bands involved in optical transitions and separated by $\hbar\omega$ as

$$\alpha_{\mathrm{OJL}}(\hbar\omega)=D^2(\hbar\omega)\,\mathcal{J}_{\mathrm{OJL}}(\hbar\omega)=\frac{1}{\hbar\omega}\frac{\sqrt{2}m_{\mathrm{c}}^{*3/2}}{\pi^2\hbar^3}\frac{\sqrt{2}m_{\mathrm{v}}^{*3/2}}{\pi^2\hbar^3}\Im(\hbar\omega) \tag{28}$$

where $\Im(\hbar\omega)$ was referred to as the *normalized* JDOS function, used to facilitate analysis, and was defined as

$$\Im(\hbar\omega) = \frac{\pi^2\hbar^3}{\sqrt{2}m_c^{*3/2}}\frac{\pi^2\hbar^3}{\sqrt{2}m_v^{*3/2}}\mathcal{J}_{OJL}(\hbar\omega) \tag{29}$$

The OJL analysis of the *normalized* JDOS $\Im(\hbar\omega)$ function has been proceeded for two photon-energy regimes for both of the cases $\gamma_c \neq \gamma_v$ and $\gamma_c = \gamma_v = \gamma$; one regime corresponds to the extended-state-to-extended-state optical transitions for photon energies $\hbar\omega \geq E_{g0} + (\gamma_c + \gamma_v)/2$ and the other accounts for optical absorption resulting from radiation-induced electronic transitions when $\hbar\omega \leq E_{g0} + (\gamma_c + \gamma_v)/2$, where $E_{g0} + (\gamma_c + \gamma_v)/2$ denotes the mobility bandgap energy. The OJL expressions of the *normalized* JDOS $\Im(\hbar\omega)$ function for the case of $\hbar\omega \leq E_{g0} + (\gamma_c + \gamma_v)/2$ are

$$\Im(\hbar\omega) = \frac{\gamma_c^2}{\sqrt{2e}}\exp\left(\frac{\hbar\omega - E_{g0}}{\gamma_c}\right)\mathcal{Y}\left(\frac{\gamma_v}{2\gamma_c}\right) + \frac{\gamma_v^2}{\sqrt{2e}}\exp\left(\frac{\hbar\omega - E_{g0}}{\gamma_v}\right)\mathcal{Y}\left(\frac{\gamma_c}{2\gamma_v}\right)$$
$$+ \frac{1}{2\sqrt{e}}\frac{(\gamma_c\gamma_v)^{3/2}}{\gamma_v - \gamma_c}\left[\exp\left(\frac{\hbar\omega - E_{g0} - \frac{\gamma_c}{2}}{\gamma_v}\right) - \exp\left(\frac{\hbar\omega - E_{g0} - \frac{\gamma_v}{2}}{\gamma_c}\right)\right] \tag{30}$$

The function $\mathcal{Y}(z)$ is given in terms of the complementary error function $\text{erfc}\,(x)$ as described below

$$\mathcal{Y}(z) = \int_z^\infty \sqrt{x}\exp(-x)dx = \sqrt{z}\exp(-z) + \frac{\sqrt{\pi}}{2}\,\text{erfc}\left(\sqrt{z}\right) = \sqrt{z}\exp(-z) + \int_z^\infty \exp(-x^2)dx \tag{31}$$

For $\gamma_c = \gamma_v = \gamma$, the first two terms of Equation (30) remain unchanged, while the third term $\Im_{3rd}(\hbar\omega)$ reduces to (O'Leary et al., 1997)

$$\Im_{3rd}(\hbar\omega) = \frac{\gamma}{2e}\exp\left(\frac{\hbar\omega - E_{g0}}{\gamma}\right)(\hbar\omega - E_{g0} + \gamma) \tag{32}$$

The OJL expressions of the normalized JDOS $\Im(\hbar\omega)$ function for the case of $\hbar\omega \geq E_{g0} + (\gamma_c + \gamma_v)/2$ are

$$\Im(\hbar\omega) = \frac{\gamma_c^2}{\sqrt{2e}}\exp\left(\frac{\hbar\omega - E_{g0}}{\gamma_c}\right)\mathcal{Y}\left(\frac{\hbar\omega - E_{g0}}{\gamma_c} - \frac{1}{2}\right) + \frac{\gamma_v^2}{\sqrt{2e}}\exp\left(\frac{\hbar\omega - E_{g0}}{\gamma_v}\right)\mathcal{Y}\left(\frac{\hbar\omega - E_{g0}}{\gamma_v} - \frac{1}{2}\right)$$
$$+\left(\hbar\omega - E_{g0}\right)^2\Upsilon\left(\frac{\gamma_c}{2(\hbar\omega - E_{g0})}, \frac{\gamma_v}{2(\hbar\omega - E_{g0})}\right) \tag{33}$$

The function $\Upsilon(x, y)$ is defined by the following integral (O'Leary et al., 1997)

$$\Upsilon(x, y) = \int_x^{1-y}\sqrt{z}\sqrt{1-z}\,dz \tag{34}$$

In the disorderless limit $\gamma_c \to 0$ and $\gamma_v \to 0$, the OJL interband transition model reduces to Tauc model with $\epsilon''_{OJL}(\hbar\omega) \to 0$ for $\hbar\omega < E_{g0}$ and $\epsilon''_{OJL}(\hbar\omega) \to \alpha_{Tauc}(\hbar\omega) \propto \left(\hbar\omega - E_{g0}\right)^2$ for $\hbar\omega \geq E_{g0}$. But, $\epsilon''_{OJL}(\hbar\omega)$ rises to infinity as $\omega \to \infty$, as in Tauc model, which is unrealistic from practical viewpoint (Theiss, 2012; Jellison & Modine, 1996) and which is not desired when the real part $\epsilon'_{OJL}(\hbar\omega)$ of complex dielectric constant of a disordered amorphous semiconductor is calculated from Kramers-Kronig relations (KKR).

3. Experimental Details

Undoped selenium (Se) films of various thicknesses were deposited at a rate of $2 - 5$ Å/s by thermal evaporation under working vacuum of ~ 5 x 10^{-5} mbar onto well chemically-treated and cleaned 1.1-mm thick soda-lime glass slides held at 28 ℃ ($\pm$ 1 ℃), below glass-transition temperature of undoped selenium. Selenium target used in the evaporation of films was taken from as-purchased commercial selenium pellets (Analytical Reagent (AnalaR), BDH Chemical Ltd., England) without further purification. The as-deposited Se-films were stored in a dark humidity-free desiccator, prior to taking structural and optical measurements on them, to reach structural relaxation equilibrium and to impede possible glass transformation. The geometric thickness d of the films was monitored in-situ thru evaporation by a quartz-crystal installed in the chamber of deposition system. Several replicas of Se-films were produced with $=$ 0.25 μm, 0.5 μm, 0.75 μm, and 1 μm. The as-deposited Se films were all pinhole-free and had smooth surfaces without traces of cracks. The structure and surface morphology of as-deposited Se-films were studied at room temperature by X-ray diffraction (XRD) and scanning electron microscopy (SEM) techniques, the results of which revealed their amorphous structure, in good agreement with XRD diffractograms and SEM micrographs of Se-films prepared in our laboratory under same conditions (Abdul-Gader et al., 1998; Abdul-Gader & Nigmatullin, 2001; Al-Hamarneh et al., 2009). We designate the

sample made of a thin Se film deposited onto a thick glass slide and standing freely in air by a *four-layered* structure with the {air/thin Se-film/thick glass slide/air}-stacking, air-supported *bare* glass slide by a *three-layered* structure of {air/slab/air}-stacking, and label the four-layered structures of the 0.25-μm, 0.5-μm, 0.75-μm and 1-μm thick amorphous selenium films grown at 28 ℃ by Se250, Se500, Se750, and Se1000, respectively. The normal-incidence transmittances $T_{\exp}(\lambda)$ of a typical 1.1-mm thick air-supported glass-slide and of air-supported selenium four-layered structures were measured at room temperature as a function of spectral wavelength λ in the range 300-1100 nm. Transmittance measurements were made using a double-beam SPECORD® UV-Vis-NIR spectrophotometer (Analytik Jena AG Model 210) at a scan rate of 120 nm/min with a narrow spectral bandwidth (SBW) ($\leq$ 4 nm) to avoid shrinking of interference-fringe pattern of as-measured $T_{\exp}(\lambda) - \lambda$ spectra (Tan, 2006; Tan et al., 2007; Tan et al., 2006; Swanepoel, 1984; Bennouna et al., 1992; Márquez et al., 1995; Ruíz-Pérez et al., 2001; Márquez et al., 1999; Pradeep & Agarwal, 2010; Richards, 1998; Richards et al., 2004) and to have good signal-to-noise ratio. Both of the $T_{\exp}(\lambda) - \lambda$ spectra of the studied {air/thin *a*-Se-film/thick glass-slide/air}- and {air/thick glass-slide/air}- samples were recorded relative to a corrected air-baseline, where the transmittance of air was recorded with both light-beam paths were free from any sample and then normalized to 100%. Transmittance measurements were then taken with the studied sample being placed in its light-beam path, leaving the reference light-beam path uncovered.

4. Results and Discussion

Figure (3) depicts the *as-measured* room-temperature normal-incidence specular transmittance $T_{\exp}(\lambda)$ of typical Se250, Se500, Se750, and Se1000 samples and of a representative air-supported 1.1-mm thick glass slide as a function of the spectral wavelength λ in the range 300 – 1100 nm. Before executing curve-fitting (simulation) of the experimental $T_{\exp}(\lambda) - \lambda$ data of such samples to theoretical $T_{\text{theor}}(\lambda)$-formulation to extract optical constants of their *a*-Se films, it is worthy to discuss several appealing features of their transmittance spectra, though transmittance is not in itself an intrinsic property of the material from which the film is made.

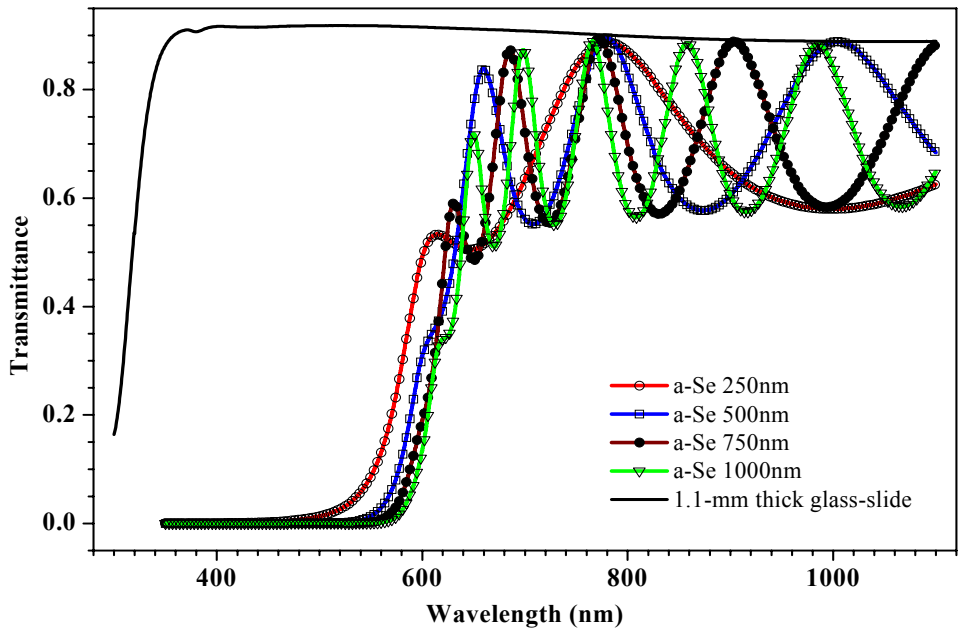

Figure 3. Normal-incidence $T_{\exp}(\lambda) - \lambda$ spectra of Se250, Se500, Se750, and Se1000 samples. The dark solid curve depicts normal-incidence transmittance of a 1.1-mm thick glass slide standing freely in air measured at room temperature

Firstly, the as-measured $T_{\exp}(\lambda) - \lambda$ curves of the studied air-supported {*a*-Se film/glass substrate}-samples exhibit well-resolved interference-fringe extremes (maxima and minima) in the wavelength range 650-1100 nm. The number of observed interference maxima and minima increases and their spectral widths become smaller (closely spaced) with increasing geometric thickness of the deposited selenium film. The transmittance interference-fringe regions will be hereafter referred to as the transparent, weak and medium optical absorption regions.

Secondly, the *a*-Se film and its substrate are transparent in the region where absorption in both is feeble, with their extinction coefficients κ_s and κ are zero and the film's absorption coefficient $\alpha\ (\equiv 4\,\pi\,\kappa/\lambda) \cong 0$, so the transmission of an {air/undoped *a*-Se-film/glass substrate/air}-structure is only determined in this spectral region by n and n_s, the indices of refraction of film and substrate, respectively. In the transparent region, the value of *as-measured* normal-incidence *maximum* transmittance T_{M0} of each air-supported {*a*-Se-film/glass substrate}-sample is clearly approaching the practically constant as-measured optical transmittance $T_s(\lambda)$ of an *air-supported glass slide*, which is described by Equation (A29) that is valid for insignificant absorption in this glass substrate. With a little algebra, one can obtain that Equation (A29) is equivalent to the T_{M0}-formula given in Equation (A28) by putting $x \equiv \exp(-\alpha d) \cong 1$- that is, there is insignificant optical absorption in the *a*-Se film in this transparent region, suggesting good consistency between theory and experiment.

Thirdly, the departure of the amplitudes T_{M0} of the observed maxima fringes on the transmittance curve of any studied air-supported {*a*-Se-film/glass substrate}-stack from the nearly constant experimental transmittance of its glass substrate is significant in its medium absorption region compared with that observed in its transparent and weak absorption regions. This behavior can be ascribed to progressive optical absorption of light waves traversing back and forth inside the *a*-Se film, and *not to shrinking* of the observed interference-fringe maxima and minima overlaid on as-measured transmittance spectra of its sample. Interference-fringe shrinkage is seen in as-measured transmittance (reflectance) of non-uniform and inhomogeneous films or when optical measurements are made using pseudo-monochromatic light of large SBWs (Tan, 2006; Nagels et al., 1997).

However, shrinking of interference-fringe maxima and minima are not so obvious from the *as-measured* transmittance of our samples even those integrating thick selenium films; in view of the justifiable model approximations underlying the numeric curve-fitting procedures, this would have no vital influence on the fit results, yet it cannot be entirely excluded as extra physical parameters of air-supported {Se-film/thick substrate}-stacks can be found (Nagels et al., 1997). Such features of the as-measured transmission spectra of undoped *a*-Se films laid on thick glass slides motivated us to treat them as thin films with good thickness uniformity, homogeneity, and smooth, roughness-free and plane-parallel surfaces. Also, their glass-slide substrates were transparent with nearly constant transmittance in the wavelength range 360-1100 nm and assume that the used spectrophotometer's SBW to be reasonable with minor effect on their as-measured optical transmission. Otherwise, we had to analyze these $T_{exp}(\lambda) - \lambda$ spectra by taking into account possible shrinkage of their interference-fringe patterns, which for small SBWs might originate from non-uniformity in the geometric thickness of the *a*-Se film and from roughness over its surfaces (Tan, 2006; Nagels et al., 1997). Analysis of as-measured transmittance spectra of these air-supported {*a*-Se/glass-substrate}-samples can be completed by including the spectral dispersion of the substrate's index of refraction and influence of absorption inside substrate over the wavelength range of interest.

Fourthly, all as-measured $T_{exp}(\lambda) - \lambda$ curves of our Se250, Se500, Se750, and Se1000 samples start, below the wavelength $\lambda_C \sim 635$ nm, to decline, slightly smeared, towards zero transmittance, where λ_C signifies the border for the absorption edge of the film's material, which for undoped *a*-Se is well above that of soda-lime glass ($\lambda_C \sim 350$ nm). The interference-fringe patterns are noted to disappear in strong absorption region for all these {air/thin *a*-Se-film/thick glass-slide/air}-samples, with optical transmissions being exclusively determined by the absorption coefficient α of their selenium films. In practice, α of a thin absorbing film of geometric thickness d is in general very large in the strong optically absorbing region ($\lambda < \lambda_C$), so that the absorbance parameter $x \equiv \exp\ (-\alpha\ d) \ll 1$. This model approximation is helpful when discussing the physics of transmittance spectra of semiconducting films in their strong absorption regions, where a drop in their transmission curves with decreasing wavelength should be observed. The absence of sharp but smeared transmission of these undoped *a*-Se samples at wavelengths lower than λ_C can be related to the presence of native and disorder structural defects and imperfections, a feature that is often observed for amorphous films, in contrary to the abrupt fall in transmission spectra of pure and perfectly crystalline films that occurs at a definite wavelength λ_C, which is an inherent (intrinsic) characteristic of the material itself.

Optical absorption in a semiconducting sample may be ascribed to photon-induced electronic transitions from extended valence-band energy states to extended empty conduction-band energy states and/or from extended valence-band energy states to the bandgap localized states below conduction band, or from bandgap localized energy states above valence-band edge to localized energy states below conduction-band edge, depending on its crystallinity, purity and quality (Theiss, 2012; O'Leary et al., 1997; Dias da Silva et al., 2004). The physics of optical behavior of materials associated with electronic transitions and dielectric mechanisms, together with their formulations are discussed in Appendix B and section (2). More details on this issue can be found in a variety of books of solid state physics and optics, and literature reviews (Tauc, 1972; Tauc, 1979; Heavens, 1991; Azzam &

Bashara, 1987; Ward, 1994; Dragoman & Dragoman, 2002; Stenzel, 2005; Joo et al., 1999; Theiss, 2012; Forouhi & Bloomer, 1986; Forouhi & Bloomer, 1988; Adachi, 1991; Jellison & Modine, 1996; Chambouleyron & Martínez, 2001; Truong & Tanemura, 2006; Kasap & Capper, 2006; Christman, 1988; Rogalski & Palmer, 2000; Palik, 1998; Dressel & Grüner, 2002; Reitz et al., 1993). Since transmittance is not an intrinsic property of material, further quantitative analysis of $T_{\exp}(\lambda) - \lambda$ spectra of our air-supported {*a*-Se film/thick glass substrate}-samples is needed to retrieve optical constants $n(\lambda)$ and $\kappa(\lambda)$ ($\equiv \lambda\, \alpha(\lambda)/4\pi$) of their Se-films, their spectral dispersion functions, and to elucidate electronic transitions responsible for optical absorption in such films. Of the various analytical and numeric optical approaches used to analyze transmittance and/or reflectance spectra of a film's structure to achieve these objectives, we have analyzed the $T_{\exp}(\lambda) - \lambda$ data of our thermally-evaporated *a*-Se films grown on thick glass slides by a recent SCOUT version (3.77), combined with apt dispersion function models to retrieve their geometric thicknesses and spectral dispersion of their optical constants.

4.1 Modeling of Specular Transmittance Spectra of a-Se Films Laid On 1.1-mm Thick Glass-Slide Substrates

To extract the dispersion of dielectric and optical constants of our air-supported {*a*-Se/microscopic glass-slide}-samples, the SCOUT software (version 3.77) was utilized to curve fit their as-measured normal-incidence $T_{\exp}(\lambda) - \lambda$ spectra to theoretical formulas of specular transmittance of four-layered structures having the {air/thin film/thick substrate/air}-stack, with the film being considered either flat and uniform or when it suffers from some inhomogeneity and surface roughness. This simulation procedure cannot be achieved unless one inserts in the theoretical expression a combination of dielectric function models that would describe optical response of the film under study. A large number of dielectric models are installed in the database of SCOUT windows software, which proves to be a powerful curve-fitting program for analyzing optical spectra of multi-layered structures by comparing theoretical specular transmittance $T_{\text{theor}}(\lambda)$- and reflectance $R_{\text{theor}}(\lambda)$- formulas with $T_{\exp}(\lambda)$ and $R_{\exp}(\lambda)$ measurements. This is realized by inserting the dielectric functions to model the overall macroscopic complex electric susceptibility $\hat{\chi}(\omega) \equiv \chi'(\omega) + j\chi''(\omega) \equiv \hat{\epsilon}(\omega) - 1$ of the structure's film, arising from different dispersion and loss mechanisms, depending on its microstructure, disorder, purity, and quality.

A single dielectric function may not be ample to model $T_{\exp}(\lambda) - \lambda$ spectra of an air-supported {film/glass substrate}-stack, and a combination of dielectric functions would be more representative. The effect of dispersion and absorption in various types of substrates is taken into account in SCOUT software, where optical constants of microscopic glass slides, for example, are modeled by a set of several Kim harmonic oscillators (Theiss, 2012). Theoretical formulas of specular transmittance of multi-layered structures are introduced in the SCOUT software via a Matrix form, which involve optical constants $n(\omega)$ and $\kappa(\omega)$ of its layers (see Appendix A), with $n(\omega)$ and $\kappa(\omega)$ being calculated in-situ via the formulas relating them to the effective macroscopic complex dielectric constant $\hat{\epsilon}(\omega)$ (see Equations (B4) to (B6) in Appendix B).

4.2 Procedure of Executing SCOUT Software to Get the Required Simulated Optical Spectra

The main steps for curve-fitting (simulation) of an experimental transmittance spectrum of a multi-layered structure, for instant, by SCOUT software are illustrated by the flowchart in Figure (4) and briefed below.

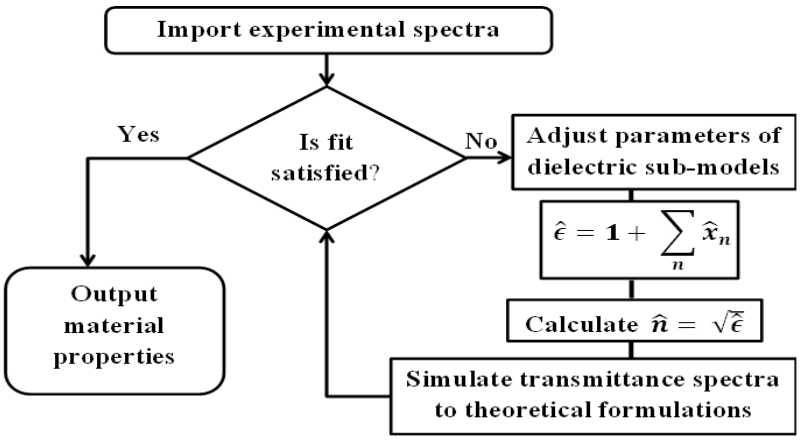

Figure 4. Flowchart for curve-fitting (simulation) of measured transmittance spectra by the SCOUT software

Let us review the main steps used to execute SCOUT software to attain curve-fitting (simulation) of as-measured normal-incidence transmittance spectra of our air-supported (a-Se film/thick glass-slide substrate}-samples. The measured $T_{\exp}(\lambda) - \lambda$ data to be simulated was first imported to a workbook in the SCOUT software and is plotted on a window chart. The type of materials comprising this layered structure is then specified in a geometric structure showing the scheme of stack layers in sequence: semi-infinite vacuum layer, material of thin film (a-Se), thin roughness layer (if exists), substrate material (glass slide), then a semi-infinite vacuum layer, with initial values for the thickness of material layers. Optical constants of the glass slide are imported from the database of SCOUT software. Then, the spectral range (nanometer or wavenumber) of the data is specified, including start and end measured data points, together with the number of points used in the fit curve. Next, select dielectric (dispersion) models, via their respective susceptibility terms, for adjusting optical constants of the selenium film to fit (simulate) its experimental transmittance data to adopted theoretical formulations. The studied thermally-evaporated selenium films were amorphous and may suffer from structural disorder leading to the creation of imperfections and lattice defects in them, which, in turn, modify their energy band structures and result in a spread of localized energy states in the bandgap of the semiconductor (band-tailing energy states).

Modeling of as-measured transmittance (reflectance) spectra of amorphous semiconducting films may be achieved by a combination of Lorentz harmonic oscillator (LHO) dielectric functions (or modified versions) and/or Drude-like dispersion models, the formulations of both incorporate explicitly the real and imaginary parts of the complex electric susceptibility; thus, no need to use Kramers-Kronig (KK) integral dispersion relations. Further, modeling of experimental transmittance spectra of such films can also be attained by making use of the combined Tauc-Lorentz (Jellison-Modine) or OJL interband transition models, which give rise to only the imaginary part of the dielectric constant (electric susceptibility) of the sample and, in the SCOUT software, the formulations and procedures of which are inserted under the KK susceptibility model list. The KK relation is then used to calculate the real part of the dielectric function from a fairly large number of data points, where no resolution hitches are confronted in the ultraviolet and visible regions, but may be encountered in the infrared, as SCOUT simulation of measured data is performed using wavenumbers $\bar{\nu}$ ($\equiv 1/\lambda$). After that, select the film thickness and constant parameters of the dielectric models chosen for curve-fitting by the SCOUT software, together with intervals of their minimum and maximum values, over which they can be adjusted to achieve optimal consistency between simulated curves and measured data. The fit procedure can be implemented manually, visually, and/or automatically in the sense that the parameters of the adopted dielectric model (s) and other fit parameters initially selected can now be varied manually, by typing new values, or visually, by the use of mouse-driven sliders that can be constructed nearby the window screen plots, before running the program automatically with the optimization method being adopted in the SCOUT software, which is (in version 3.77) a familiar method known as the downhill simplex minimization technique (Theiss, 2012; Press et al., 1992).

4.3 Adopted Dielectric Models for Air-Supported {a-Se Film/Glass Slide}-Stacks and Their Simulation Spectra

As the spectral dispersion of optical constants of glass substrates of our undoped a-Se films can be taken from SCOUT database and inserted in theoretical transmittance formulations, we need only to choose the dielectric models that my describe properly the observed optical response of these a-Se films, in which we presume that structural disorder with defects, imperfections and bandgap (Urbach) tails of localized energy states exist. As their specular transmittances were measured in a wavelength range (300 – 1100 nm), below the infrared, Drude-like dispersion models were abandoned from present optical analysis, because free charge-carrier (*intraband transitions*) effects are expected to be negligible in undoped or slightly-doped semiconductors in the visible and ultraviolet regions of electromagnetic spectrum.

First, we tried to model as-measured transmittance spectra of our air-supported {a-Se film/glass substrate}-samples by making use of a single or combination of Lorentz dielectric models as well as of their modified versions in conjunction with a constant index of refraction n_∞, inserted to compensate for dielectric contributions at wavelengths smaller than studied, in addition to implementing in some runs inhomogeneous roughness overlayer on the surface of selenium film. Surface microroughness layer were introduced within the Bruggeman effective-medium (BEM) approximation to account for scattering losses from the film surface. But, combination of Lorentz-like dielectric dispersion models with or without surface roughness gave bad fits for as-measured transmittance data of our undoped a-Se samples, though a combination of two LHO models has been employed by Navarrete et al. (1990) to curve fit normal-incidence transmittance spectra of their undoped a-Se films. We believe that Lorentz dielectric model is not adequately workable in the interband transition region of disordered amorphous semiconductors. Next, a Tauc-Lorentz model modified with a Heaviside step function (see formulas in SCOUT manual) was also found to give rather unacceptable curve fits for the transmittance data of our a-Se films in the studied spectral range, where it seems to work properly in the interband transition region of

defect-free, crystalline substances (Innami et al., 1999; Adachi, 1991; Jellison & Modine, 1996). Yet, Innami et al. (1999) reported that a combination of four-term Tauc-Lorentz functions can model ellipsometric measurements made on thermally-evaporated *a*-Se films in the spectral energy range 1.2- 5.2 eV.

Since the selenium films studied in this work were undoped, amorphous and may contain native (intrinsic) defects, we have supposed that there were some localized energy states spread in the bandgap of amorphous semiconducting selenium, and hence the presence of band tails of energy states below the edges of its conduction and valence bands. The effect of band tails on the absorption spectra of an amorphous and disordered semiconductor in its interband transition region is not explicitly taken into account in Tauc-like formulations of optical absorption or in the Tauc-Lorentz dielectric model. On the other hand, the OJL interband transition model formulations take into account the influence of band tails in the form of exponential-like functions in optical absorption of a disordered amorphous semiconductor (Solieman & Abu-Sehly, 2010; Theiss, 2012; O'Leary et al., 1997; Dias da Silva et al., 2004). Therefore, we have employed the OJL interband transition model to fit the entire as-measured normal-incidence transmittance $T_{\mathrm{exp}}(\lambda) - \lambda$ data of these air-supported {*a*-Se film/glass substrate}-samples to the full theoretical formulas that describe specular transmittance $T_{\mathrm{theor}}(\lambda)$ of an ideal {air/thin film/thick substrate/air}-stack (see Appendix A for details).

The OJL interband transition model incorporates closed-form analytical expressions for the absorption coefficient $\alpha(\omega)$ or for the imaginary part $\epsilon''(\omega)$ of complex dielectric constant $\hat{\epsilon}(\omega)$ of the sample and not its real part $\epsilon'(\omega)$. Further, the OJL model yields $\epsilon''(\omega) > 0$ for photon energies $\hbar\omega$ less than the semiconductor's absorption edge, but with $\epsilon''(\omega)$ increases to infinity with increasing photon energy to infinity due to its strong dependence on the joint density of state (JODS); however, both experimental and theoretical findings indicates that $\kappa(\omega)$ goes to 0 as $\hbar\omega \longrightarrow \infty$. This limit is of particular importance in the evaluation $\epsilon'(\omega)$ from $\epsilon''(\omega)$, or vice versa, using KK integrals. In practice, there are some restrictions and requirements on performing KK- ϵ' (ϵ'') integrals. Both $\epsilon'(\omega)$ and $\epsilon''(\omega)$ functions must be valid, or their numeric data are known, over a very wide spectral range, from $\omega = 0$ to $\omega = \infty$. To evaluate $\epsilon'(\omega)$ using KK-relations, the condition $\epsilon''(\omega \to \infty) \to 0$ must be fulfilled, which is not explicit in the OJL $\epsilon''(\omega)$-formula, in addition to the fact that there are no real transmittance or reflectance data that can be measured for all frequencies in the range $0 \leq \omega \leq \infty$. A finite maximum frequency instead of infinity can be acceptable only in evaluating $\epsilon'(\omega)$ from KK relations if the imaginary part $\epsilon''(\omega)$ smoothly approaches zero at the high-frequency side. The KK relations in SCOUT software are used with certain number of data points (256, 512, 1024, 2048,4046, 8192, 16384), as it utilizes two successive Fourier transforms; a Fast Fourier Transforms (FFT) program that is limited to these restricted number of data points to transform $\epsilon''(\omega)$ to $\epsilon'(\omega)$. A rather limited number of data points less than 2048 can be used with reasonable spectral resolution ($\leq 100\ \mathrm{cm}^{-1}$) when the KKR dielectric function models are computed for wavelengths in the UV-Vis-NIR regions, where interband transitions in most semiconductors takes place, but runs into sever difficulties with this resolution when describing infrared vibrational modes (Theiss, 2012). The $\epsilon''(\omega)$-formulation of the original OJL interband transition model has been modified in the SCOUT software by multiply the OJL $\epsilon''(\omega)$ -expression by an empirical exponential-like functional term given, in units of wavenumbers, by the functional factor $\exp\{-[[(\gamma(\mathrm{cm}^{-1}) - E_{\mathrm{g0}}(\mathrm{cm}^{-1})]/\mathrm{Decay}\ (\mathrm{cm}^{-1})]^{1/2}\}$, where Decay-term is a non-zero parameter, to drag down the imaginary part $\epsilon''(\omega)$ to zero for high frequencies, and the other symbols have their usual meaning in the OJL model.

In the SCOUT software the KKR dielectric function models are introduced in the object of type "dielectric function model" within a list called KKR susceptibility which makes use of KKR dielectric function model internally, not in the list of materials directly. Using KKR dielectric function models in this way one can mix the complex susceptibility functions that require KKR construction of the real part with those have explicit expressions forms- that is, "normal susceptibility terms" for the real and imaginary parts for $\epsilon'(\omega)$ and $\epsilon''(\omega)$. All KKR susceptibilities are being first summed up and then used to compute the corresponding real part, to which all the "normal susceptibility terms" that do not require a KKR transformation added (Theiss, 2012). Also, a constant susceptibility term was added via the use of a real constant index of refraction n_{∞}, the square of which is the real part of susceptibility whose imaginary part is zero. This term is introduced to account for contributions to dielectric susceptibility of the semiconductor from loss processes and excitations in the infrared far away from region of interband transitions- that is, a dielectric background.

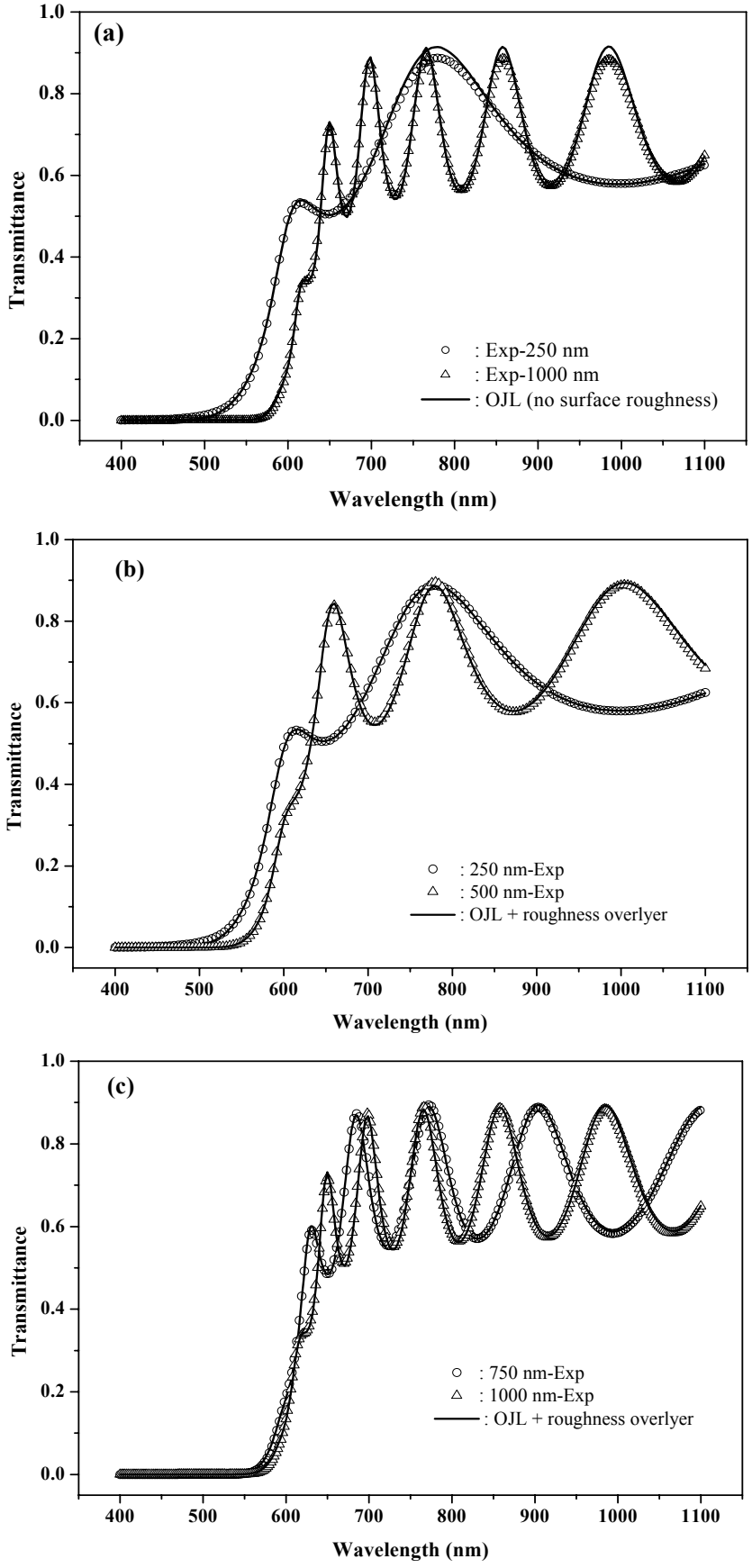

Figure 5. Curve fits (lines) of OJL interband transition model plus n_∞, with and without roughness layer, alongside with as-measured normal-incidence $T_{\exp}(\lambda) - \lambda$ data (symbols) of air-supported {a-Se film/glass substrate}-samples

At first stage, the modified OJL $\epsilon''(\omega)$ in conjunction with n_∞, with and without surface roughness layer, were used within the KKR susceptibility, to simulate as-measured $T_{\exp}(\lambda) - \lambda$ spectra of our Se250, Se500, Se750, and Se1000 samples. We found that a combination of a modified OJL model plus a constant susceptibility is suitable to model $T_{\exp}(\lambda) - \lambda$ spectra, but the obtained $T(\lambda) - \lambda$ curve-fits depart marginally from their respective as-measured $T_{\exp}(\lambda) - \lambda$ curves; yet, the insertion of a thin roughness layer δd with microstructure inhomogeneity over the surface of studied selenium films (within Bruggeman effective-mean approximation) yielded noticeable consistency between simulation and measured spectra as depicted in Figure (5), though our *a*-Se films looked to be fairly uniform in thickness, smooth, homogeneous and cluster-free (as inferred from their as-measured transmittance spectra rich in well-resolved interference fringes and high-resolution SEM micrographs). The effect of such artifacts cannot always be excluded from analysis of as-measured optical response of undoped *a*-Se films deposited onto thick glass slides (Nagels et al., 1997).

The obtained SCOUT simulation values of fit parameters of adopted Lorentz and OJL dielectric models are listed in Table (1) and seem to be physically meaningful and representative for *a*-Se. The effect of fit parameters γ_c and γ_v in the OJL interband transition model describing spread of valence and conduction bands tails of energy states in bandgap is significant, but not large (40 meV to 50 meV), implying that some structural and disorder imperfections were present in studied as-deposited undoped *a*-Se films. The fit bandgap energy E_0 in the OJL interband transition model has values ranging between 1.9 eV and 2 eV, with little dependence on film thickness, in good agreement with other literature findings (Tan, 2006; Tan et al., 2007; Tan et al., 2006; Kotkata et al., 2009; Nagels et al., 1997; Innami et al., 1999). The fit values of $n_\infty = \sqrt{\epsilon_\infty}$ were in the range 1.9 - 2.1, in good agreement with $\epsilon_\infty = 4.8$, the high-frequency contribution to dielectric constant found by Navarrete et al. (1990) that is, as expected, less than those of long-wavelength (zero-energy) dielectric constant around 6 deduced from other measurements on undoped *a*-Se films using different analytical approaches (Nagels et al., 1997; Innami et al., 1999). The geometric thicknesses d of our *a*-Se films retrieved from SCOUT curve-fits are in harmony with but always systematically higher than those recorded during film growth (within an uncertainty of $\Delta d \cong 15\%$), and with the results obtained from a comprehensive analysis carried out using the PUMA program and the analytical envelope method of Swanepoel (results will be published elsewhere). It is worth noting here that if global minima were achieved in SCOUT curve-fitting of $T_{\exp}(\lambda) - \lambda$ data of air-supported {*a*-Se film/glass substrate}-samples, the resulting simulated $T(\lambda) - \lambda$ curves and fit parameters were reproducible upon inserting physically meaningful initial values for them; otherwise bad fits and unreliable values were often obtained.

Table 1. Best fit parameters of an OJL interband-transition model plus n_∞ used to simulate measured room-temperature normal-incidence transmittance spectra of the studied undoped *a*-Se samples. The retrieved values of the geometric thickness d and surface roughness layer δd are also quoted

Dielectric model	Sample	Se250	Se500	Se750	Se1000
OJL + roughness layer	d (nm)	293	604	890	1171
	n_∞	2.1	1.96	1.98	1.93
	δd (nm)	5.2	2.3	4	3.2
	γ (meV)	40	41	44	45
	E_{g0} (eV)	1.94	1.96	1.95	1.95
	Strength	8.8	9.1	8.2	7.6
	Fit deviation	6×10^{-6}	2.5×10^{-5}	2.4×10^{-5}	2.4×10^{-5}

4.4 Retrieved Dielectric and Optical Functions of Undoped Amorphous Selenium Films

The optical and dielectric behavior of our undoped *a*-Se films can be typified by the dependence of retrieved SCOUT curve-fit real and imaginary parts of their overall complex dielectric constant $\epsilon'(\hbar\omega)$ and $\epsilon''(\hbar\omega)$ on the exciting photon energy $\hbar\omega$. For purposes of comparison with literature findings (Adachi & Kao1980; Kotkata & Abdel-Wahab, 1990; Kotkata et al., 2009; Innami et al., 1999), the dielectric constants of these *a*-Se films are shown in Figure (6a) as a function of wavelength λ. *First*, it is clear that there is only a slight change in the magnitude and peak value of electric susceptibility of our undoped *a*-Se films with thicknesses above 250 nm, in fair agreement with SCOUT curve-fit results found by Solieman et al. (2010) on undoped *a*-Se films of reduced thicknesses. *Second*, $\epsilon'(\lambda)$ shows a peak at a wavelength near 0.53 μm which is close to that reported by Adachi and co-workers (Adachi & Kao1980; Innami et al., 1999), whereas $\epsilon''(\lambda)$ shows a trend towards a maximum value at $\lambda \sim 0.42$ μm, which is in excellent consistency with the results of Adachi and Kao (1980) but not with other literature findings (Solieman & Abu-Sehly, 2010). In case of *a*-Se this is mainly attributed to onset of optical

absorption due to photon-induced electronic transitions from filled states in valence band to empty states in conduction band, perhaps a band-to-band UVB → LCB transitions occurring for photon energies larger than 1.9 eV ($\lambda < 600$ nm) (Innami et al., 1999)- that is, in the visible region far above frequencies where free charge-carrier or ionic resonances take place.

The optical behavior of these undoped *a*-Se films can be also illustrated via wavelength dependency of their optical constants $n(\lambda)$ and $\kappa(\lambda)$, whose values were calculated in the SCOUT software from the best fit values of the overall (effective) complex electric susceptibility of the adopted combined dielectric models using the formulations of Equations (B4) to (B6). The retrieved $n(\lambda) - \lambda$ and $\kappa(\lambda) - \lambda$ data for these undoped *a*-Se films are illustrated in Figure (6b), where in the spectral region below absorption edge of undoped selenium the extinction coefficient $\kappa(\lambda)$ is almost zero and the index of refraction is dispersive and marginally dependent on film thickness above 250 nm, in fair agreement with other findings on undoped *a*-Se films (Solieman & Abu-Sehly, 2010). The value of $n(\lambda)$ of our undoped *a*-Se films increases monotonically from 2.5 at long wavelengths to near 3 with increasing wavelengths and then starts to decrease, with a broad peak their $n(\lambda) - \lambda$ curves can be noticed to be centered about $\lambda \sim 0.52$ μm, which can be related to the band-to-band UVB → LCB electronic transitions, in good agreement with several literature results obtained using different analytical approaches (Adachi & Kao1980; Kotkata et al., 2009; Nagels et al., 1995; Tichy et al., 1996; Nagels et al., 1997; Innami et al., 1999).

There is a trend for a peak to commence in the extinction coefficient $\kappa(\lambda) - \lambda$ curves or imaginary part of dielectric constant $\epsilon''(\lambda) - \lambda$ curves of our undoped *a*-Se films, but no clear broad peaks were obtained as much shorter wavelengths than studied seem to be needed. The spectral dependence (dispersion) of the index of refraction of the studied undoped *a*-Se films is fitted to a Sellmeier relation (Equation (B41)) or Wemple-DiDomenico relation (Equation (B42)), which describes dielectric behavior of a single-effective harmonic oscillator at long wavelengths below absorption edge. This is depicted as plots of $\{[n(h\nu)]^2 - 1\}^{-1}$-versus-$(h\nu)^2$, as shown for typical *a*-Se films of different thicknesses in Figure (6c). It is seen that there are notable curve-fit straight line portions in the long-wavelength region that deviates at shorter wavelengths (high photon energies) since such dispersion relations are valid below absorption edge of the semiconductor. The intercepts ($= E_0/E_d$) of linear portions of the $\{[n(h\nu)]^2 - 1\}^{-1}$-versus-$(h\nu)^2$ plots of Figure (6c) at $\hbar\omega = 0$ yield the static index of refraction $n_0 = n(E = 0) = \sqrt{1 + E_\mathrm{d}/E_0}$ and their slopes give $1/E_\mathrm{d}E_0$, where E_0 and E_d are, respectively, the single-oscillator "effective" energy gap and dispersion parameters in Wemple-DiDomenico model (Equation (B42)), the values of which for our undoped *a*-Se films are listed in Table (2). The obtained n_0-values lie in the range $2.4 - 2.46$, in excellent agreement with findings of other workers (Nagels et al., 1997; Innami et al., 1999). Within experimental errors, changes in index of refraction with film thickness can be accounted by changes in the film's mass density, via the Clausius-Mossotti relation (Tan, 2006; Tan et al., 2007; Tan et al., 2006).

Table 2. Values of E_0, E_d, n_0 , $E_\mathrm{g}^{\mathrm{opt}}$ and $E_\mathrm{g}^{\mathrm{linear}}$ (linear and square Tauc bandgap energies), with Γ_U (Urbach tail) obtained from least-squares fits of linear portions of the $[n^2 - 1]^{-1}$-$(h\nu)^2$, $[\alpha(h\nu)h\nu]^\mathrm{r}$-$h\nu$ ($\mathrm{r} = 1$ & $1/2$), and semi-log $\alpha(h\nu) - h\nu$ plots of undoped *a*-Se films. Fit R^2-function was better than 0.997 and the uncertainty in their extracted values was estimated to be better than ± 1%

Model	Wemple-DiDomenico plots			Tauc and Urbach-tail plots		
a-Se sample	E_0 (eV)	E_d (eV)	n_0	$E_\mathrm{g}^{\mathrm{opt}}$ (eV)	$E_\mathrm{g}^{\mathrm{linear}}$ (eV)	Γ_U (meV)
Se250	3.99	20.2	2.46	1.91	2.15	42.3
Se500	3.90	18.3	2.39	1.93	2.20	43.5
Se750	3.95	19.0	2.41	1.92	2.16	46.3
Se1000	3.90	18.8	2.41	1.92	2.16	47.7

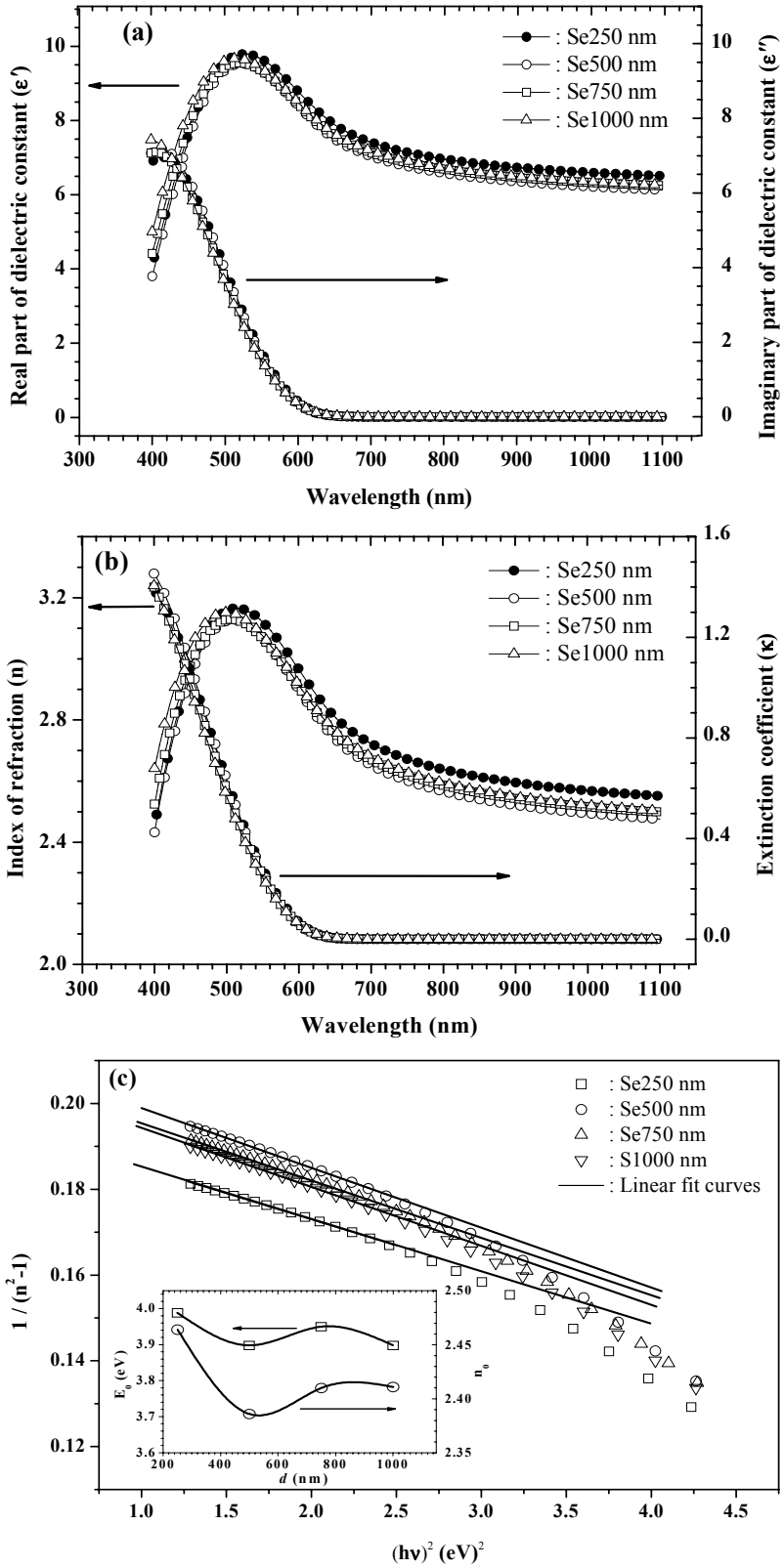

Figure 6. Dependence of **(a)** $\epsilon'(\lambda)$ and $\epsilon''(\lambda)$ and **(b)** index of refraction $n(\lambda)$ and extinction coefficient $\kappa(\lambda)$ on wavelength λ for studied undoped *a*-Se films, with solid curves are guides-to-eye and symbols are data retrieved from SCOUT curve-fits of respective transmittance spectra using the OJL model with surface roughness layer and high-frequency constant index of refraction n_∞. **(c)** curve-fits of the $\{[n(h\nu)]^2 - 1\}^{-1} - (h\nu)^2$ data for wavelengths below absorption edge on basis of Wemple-Didominco relation, where intercept with ordinate at $\hbar\omega = 0$ gives n_0 (Nagels et al., 1997). The inset to Figure (6c) depicts variation of n_0 and "effective" energy bandgap parameter E_0

The findings for the undoped *a*-Se selenium films of the present work are consistent with those reported by other workers who employed different approaches to analyze experimental (transmission and/or ellipsometric) data of their undoped *a*-Se films of alike thicknesses (Nagels et al., 1997; Innami et al., 1999). The values of the "effective" bandgap energy parameter or oscillator energy strength E_0 ($\sim 2E_g^{opt}$) and energy dispersion parameter E_d for our undoped *a*-Se films are comparable with those found by Tan et al. (2006; 2007), Nagels et al. (Nagels et al., 1997), Innami et al. (1999), and Kotkata et al. (2009), where different experimental procedures and data analysis were implemented. Our fit values of the Tauc energy E_g^{opt} and/or Urbach-tail breadth Γ_U, which are all related to the film structure and material properties, suggest that the undoped *a*-Se films of the present work had almost same amorphous structure and small structural disorder, and are also in reasonable agreement (within estimated uncertainties) with other findings on undoped and slightly-doped *a*-Se films using different experimental studies and/or analytical approaches (Tan, 2006; Tan et al., 2007; Tan et al., 2006; Vautier et al., 1988; Bettstelleret al., 1993; Mulama et al., 2014; Benkhedir, 2006; Solieman & Abu-Sehly, 2010; Nagels et al., 1995; Tichy et al., 1996; Nagels et al., 1997; Innami et al., 1999), but not consistent with the E_g^{opt}-values of other workers (Mulama et al., 2014; Kotkata & Abdel-Wahab, 1990). Kotkata et al. (2009), who employed a rather different optical analysis, reported E_g^{opt}-values for their *a*-Se films near the values obtained for our undoped *a*-Se films, but their Γ_U-values were much higher, suggesting larger structural disorder in their fabricated selenium films. It is worth noting here that the deduced fit values of E_g^{opt} (Tauc bandgap energy) is less than the mobility (extended-state) bandgap energy E_{g0} ($= E_c - E_v$) obtained from SCOUT curve-fitting of as-measured transmittance to respective theoretical formulations by an amount that depends on the extent γ_{OJL} of the band tail localized energy states (O'Leary et al., 1997; Dias da Silva et al., 2004), which is consistent with the deduced values of the Urbach-tail breadth ($\Gamma_U \sim \gamma_{OJL}$), which are somewhat less than those found for both undoped and slightly-doped amorphous selenium films (Tan, 2006; Tan et al., 2007; Tan et al., 2006; Benkhedir, 2006). It is worth noting here that there is still some controversy on the nature of band-to-band (interband) optical absorption in undoped *a*-Se, and hence on the actual value of its bandgap energy, a discrepancy that can be related to the quality of the fabricated selenium film, which largely governed by the preparation conditions, and on the model used to discuss interband electronic transitions as detailed below.

4.5 Determination of Band-Gap Energy of the Undoped Amorphous Selenium Films

To reveal physical features of band-to-band (interband) electronic transitions responsible for observed optical response of the undoped *a*-Se films of present work, the dependency of respective absorption coefficients $\alpha(\hbar\omega)$ are plotted against the photon energy $\hbar\omega$ ($\equiv h\nu$) of light incident normally onto the front surface of the film, where ν is the light frequency and $\hbar = h/2\pi$. Though a convinced debating is not yet given, the linear and square Tauc models, based on the approximate power-law $\alpha(\hbar\omega) - \hbar\omega$ formula described in Equation (20), were mainly adopted to achieve this purpose for the case of undoped *a*-Se in the interband transition region with the exponent m being either 1 or 2, depending on the exact data range used in the analysis (Mott & Davis, 1979; Tan, 2006; Tan et al., 2007; Tan et al., 2006; Vautier et al., 1988; Bettstelleret al., 1993; Mulama et al., 2014; Adachi & Kao1980; Kotkata & Abdel-Wahab, 1990; Kotkata et al., 2009; Navarrete et al., 1990; Solieman & Abu-Sehly, 2010; Nagels et al., 1995; Tichy et al., 1996; Nagels et al., 1997; Innami et al., 1999). The values of $\alpha(\hbar\omega)$ of the undoped *a*-Se films of the present work were deduced form curve-fitting of as-measured room-temperature normal-incidence transmittance spectra of their Se250, Se500, Se750, and Se1000 samples using the OJL interband transition model in conjunction with constant index of refraction n_∞ and thin roughness overlayer δd. Figure (7a) illustrates the dependency of such deduced values of $\alpha(h\nu)$ of our undoped *a*-Se films on the exciting photon energy $h\nu$ in view of these Tauc-like interband optical absorption models for disordered amorphous semiconducting samples- that is, $[\alpha(h\nu)h\nu]$-versus-$h\nu$ and $[\alpha(h\nu)h\nu]^{1/2}$-versus-$h\nu$ plots. Note first that these plots illustrate insignificant effect of film thickness on the absorption coefficient of studied selenium films. Second, the intercept of the linear portions of the two plots demonstrate that the interband (bandgap) energy associated with these linear and square power-law Tauc-like models appear to be non-matching.

To elucidate more details on the dependency of the absorption coefficient of undoped *a*-Se films studied in the present work in the sub-bandgap region, semi-log $\alpha(h\nu) - h\nu$ (Urbach-tail) plots for such films were obtained, and we present here an example of such plots for a typical 500-nm thick undoped *a*-Se film in the inset to Figure (7a). The slope, obtained from least-squares fit of the linear portion of such semi-log $\alpha(h\nu) - h\nu$ plot, gives nearly the same Urbach-tail width Γ_U ($= 40 - 50$ meV) for the studied undoped a-Se films, as one can notice from Table (2), comparable with the values of band-tail widths γ_c ($\sim \gamma_v$) of the valence and conduction bands of the studied undoped *a*-Se films that were deduced from SCOUT curve-fits of room-temperature normal-incidence transmittance spectra of their Se250, Se500, Se750, and Se1000 samples using the OJL interband transition model, together with constant index of refraction n_∞ and thin roughness layer.

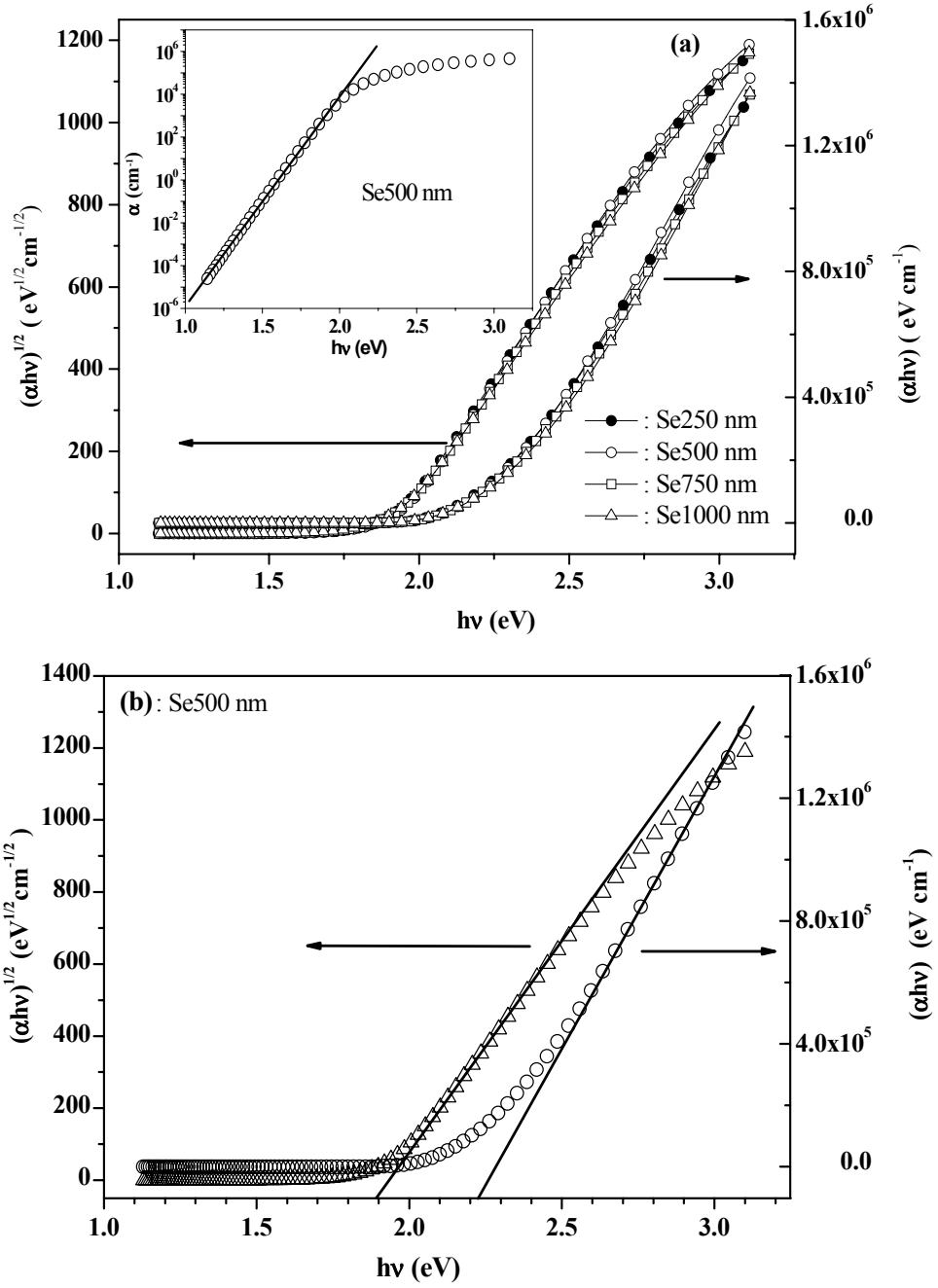

Figure 7. (a) $\alpha h\nu - h\nu$ and $(\alpha h\nu)^{1/2} - h\nu$ plots for undoped a-Se films of the Se250, Se500, Se750, and Se1000 samples, with symbols being data retrieved from SCOUT curve-fits of their normal-incidence transmittance spectra using a modified OJL interband transition model, with roughness layer and constant index of refraction n_∞. The inset shows curve fit (solid line) of the semi-log $\alpha(h\nu)$-$h\nu$ plot for the 500-nm thick undoped a-Se film, whose slope equals to Urbach-tail breadth Γ_U. (b) Least-squares fits (solid lines) of the linear portions on $\alpha h\nu - h\nu$ and $(\alpha h\nu)^{1/2} - h\nu$ plots for the 500-nm thick undoped a-Se film, the intersection of which with the $h\nu$-axis gives the respective Tauc optical bandgap energy

The linear portions of the $[\alpha(h\nu)h\nu]$-Vs-$h\nu$ and $[\alpha(h\nu)h\nu]^{1/2}$-Vs-$h\nu$ plots of the 500-nm thick undoped a-Se film shown in Figure (7b) were also least-squares fitted to Equation (20) (Tauc linear and square power-laws), the intersections of which with the $h\nu$-axis yield the respective Tauc bandgap energies E_g^{opt} and E_g^{linear} for the film, which were found to differ by about 10% (normalized to Tauc bandgap energy E_g^{opt}), the values of which are

also listed in Table (2), which shows that $E_g^{opt} \sim 1.92$ eV and $E_g^{linear} \sim 2.15$ eV, slightly dependent on film thickness (within an experimental uncertainty better than $\pm 2\%$), in remarkable agreement with few literature findings for undoped *a*-Se films (Tan, 2006; Tan et al., 2007; Tan et al., 2006; Vautier et al., 1988; Bettstelleret al., 1993; Mulama et al., 2014; Benkhedir, 2006; Kotkata et al., 2009; Solieman & Abu-Sehly, 2010 Nagels et al., 1995; Tichy et al., 1996; Nagels et al., 1997; Innami et al., 1999).

5. Conclusions and Further Suggestions

The normal-incidence specular transmittance $T_{exp}(\lambda)$ of undoped *a*-Se films of thicknesses in the range $0.25 - 1$ μm that were vacuum thermally evaporated on 1.1-mm thick soda-lime microscopic glass-slide substrates maintained at a fairly constant temperature near 28 ℃ (± 1 ℃) has been measured at room temperature as a function of spectral wavelength λ in the range $300 - 1100$ nm. Above a threshold wavelength λ_c (~ 600 nm), all as-measured $T_{exp}(\lambda) - \lambda$ spectra display transmittance values near that of glass substrates and exhibit well-resolved interference-fringe maxima and minima, signifying good uniformity of the thermally-evaporated *a*-Se films. At wavelengths less than λ_c, the $T_{exp}(\lambda) - \lambda$ curves decline gradually to zero transmittance, preceded by a fairly smeared out trend that could be related to the presence of structural disorder and defects in the fabricated *a*-Se films, which often lead to the formation of energy band tails of localized energy states in the semiconductor bandgap.

The dependency of the dielectric constant functions $\epsilon'(\lambda)$ and $\epsilon''(\lambda)$, and hence of the optical constants $n(\lambda)$ and $\kappa(\lambda)$, of the studied *air-supported* {undoped *a*-Se film/glass-slide substrate}-samples on the spectral wavelength λ were retrieved from comprehensive curve-fitting (simulation) of their $T_{exp}(\lambda) - \lambda$ data using the SCOUT software to the full theoretical $T_{theor}(\lambda)$-formulations of an *air-supported* {thin semiconducting film/thick partially-absorbing substrate}-stack via the insertion of the modified O'Leary-Johnson-Lim (OJL) interband-transition dielectric function, combined with a high-frequency dielectric constant ϵ_∞ due to dielectric background at infinite photon energy E, to model the $\epsilon'(\lambda)$ and $\epsilon''(\lambda)$ functions. Regardless of the number of observed interference fringes, reliable simulations to the as-measured normal-incidence $T_{exp}(\lambda) - \lambda$ spectra were achieved, but with somewhat marginal departure of the fit curves from experimental data. Consistency between fit curves and as-measured data has been improved when we presumed that there was a thin roughness layer ($\lesssim 5$ nm) of selenium on the top of the fabricated undoped *a*-Se films. The extracted $\epsilon'(\lambda) - \lambda$ curves showed a single broad peak around $\lambda \sim 0.52$ μm, in consistent with other literature findings, while the $\epsilon''(\lambda) - \lambda$ curves showed only a trend towards maximum. The determined $n(\lambda) - \lambda$ spectra also display a broad peak near $\lambda \cong 0.52$ μm, below which $n(\lambda)$ varies with the spectral wavelength in accordance with the Sellmeier-like (Wemple-DiDominco) single-oscillator (normal) dispersion formula, the linear least-squares fit curves of which yielded static index of refraction $n(E = 0) = \sqrt{\epsilon_s} \cong 2.42$, a dispersion energy parameter $E_d \sim 19 - 20$ eV, and oscillator "average" bandgap energy $E_o \cong 3.95$ eV $\cong 2\, E_g^{opt}$, where E_g^{opt} is the optical (Tauc) bandgap energy. Different values of E_g^{opt} and E_g^{linear} of the studied undoped *a*-Se films were deduced from linear and square Tauc-like plots and were, respectively, 1.92 eV, slightly less than fit E_{g0}-values, and 2.15 eV, while the retrieved values of the OJL band-tailing energy parameter γ were found to be in the range $40 - 50$ meV, weakly dependent on film thickness, which agree well with values of Urbach-tail parameter Γ_U signifying band tails that were deduced from least-squares of linear portions of the semi-log $\alpha(h\nu) - h\nu$ plots.

Further understanding of dielectric and optical response of undoped selenium semiconductor, and hence of its energy band structure, may be achieved if both spectrophotometric and ellipsometric measurements are made on both amorphous and crystalline films of wide-ranging geometrical thicknesses in a broad spectral range covering the UV-Vis-NIR parts of the electromagnetic spectrum. Comparison of simulation of the obtained as-measured optical data using different and reliable curve-fitting softwares that incorporate different dielectric models and other analytical and algebraic optical approaches like, for instant, the PUMA and envelope methods will be helpful and complementary.

Acknowledgements

One of authors (Mousa M. Abdul-Gader Jafar) pays gratitude to soul of the late Prof. Karel Zdansky of the Institute of Photonics and Electronics (Czech Academy of Science, Praha, Czech Republic) for his kind cooperation while taking optical measurements on the *a*-Se samples. Help of Wolfgang Theiss (W. Theiss Hard- and Software, Dr.-Bernhard-Klein-Str. 110, D-52078 Aachen, Germany) on details on the SCOUT software and its procedures is very much appreciated.

References

Abdul-Gader, M. M., & Nigmatullin, R. R. (2001). Identification of a new function model for the AC-impedance of thermally evaporated undoped selenium films using the Eigen-coordinates method. *Thin Solid Films, 396,* 282-296. http://dx.doi.org/10.1016/S0040-6090(01)01166-X

Abdul-Gader, M. M., Al-Basha, M. A., & Wishah, K. A. (1998). Temperature dependence of DC conductivity of as-deposited and annealed selenium films. *Int. J. Electron.*, *85*, 21-41. http://dx.doi.org/10.1080/002072198134328

Adachi, H., & Kao, K. C., (1980). Dispersive optical constants of amorphous Se_{1-x} Te_x films. *J. Appl. Phys.*, *51*, 6326. http://dx.doi.org/10.1063/1.327620

Adachi, S. (1991). Optical dispersion relations in amorphous semiconductors. *Phys. Rev. B, 43*, 12316. http://dx.doi.org/10.1103/PhysRevB.43.12316

Al-Hamarneh, I. F., Bulos, B. N. & Jafar, M. M. A-G. (2009). Effect of isothermal annealing and visible-light illumination on the AC-impedance behavior of undoped selenium thin films. *J. Non-Crystal. Solids, 355*, 305-310. http://dx.doi.org/10.1016/j.jnoncrysol.2008.11.006

Azzam, R. M. A., & Bashara, N. M. (1987). *Ellipsometry and Polarized light.* Amsterdam: North-Holland

Bassani, G. F., & Parravicini, G. P. (1975). *Electronic States and Optical Transitions in Solids* (Science of Solid State Monographs). Pergamon Press, chapter 5

Benkhedir M. L. (2006). Defect Levels in the Amorphous Selenium Bandgap. *PhD Thesis* Katholoieke Universiteit Leuven, Belgium

Bennouna, A., Laaziz, Y., & Idrissi, M. A. (1992). The influence of thickness and index inhomogeneities on the transmission of semiconductor thin films. *Thin Solid Films, 213*(1)*,* 55-63. http://dx.doi.org/10.1016/0040-6090(92)90474-P

Bernede, J. C., Touihri, S., & Safoula, G. (1998). Electrical characteristics of an aluminum/amorphous selenium rectifying contact. *Solid State Electron.*, *42*(10), 1775-1778. http://dx.doi.org/10.1016/S0038-1101(98)00158-0

Bettsteller R., Witte H., Herms W., & Frreistedt H. (1993) Influence of bismuth incorporation on the optical properties of a-Se films. *Solid State Comm.*, *87*(9), 763-765. http://dx.doi.org/10.1016/0038-1098(93)90409-G

Birgin, E. G., Chambouleyron, I., & Martinez, J. M., (1999). Estimation of the Optical Constants and the Thickness of Thin Films Using Unconstrained Optimization. *J. Comp. Phys.*, *151*(2), 862-880 http://dx.doi.org/10.1006/jcph.1999.6224

Born, M., & Wolf, E. (2002). *Principles of optics: Electromagnetic Theory of Propagation, Interference and Diffraction of Light* (7th edn). Cambridge: Cambridge University Press

Case, W. E. (1983). Algebraic method for extracting thin-film optical parameters from spectrophotometer measurements. *Appl. Opt.*, *22*(12), 1832-1836. http://dx.doi.org/10.1364/AO.22.001832

Chambouleyron, I., & Martínez, J. M. (2001) Optical properties of Dielectric and Semiconductor thin films in *Handbook of Thin Films Materials* (Vol. 3) *ed.* Nalwa, H. S. New York: Academic Press

Chiao, S-Ch., Bovard, B. G. & Macleod, H. A. (1995). Optical-constant calculation over an extended spectral region: application to titanium dioxide film. *Appl. Opt.*, *34*, 7355-7360. http://dx.doi.org/10.1364/AO.34.007355

Christman, J. R. (1988). *Fundamental of Solid State Physics*. Wiley & Sons, Inc.

Dias da Silva, J. H., Campomanes, R. R., Leite, D. M. G., Orapunt, F., & O'Leary, S. K. (2004). Relationship between the optical gap and the optical absorption tail breadth in amorphous GaAs. *J. Appl. Phys.*, *96*(7), 7052. http://dx.doi.org/10.1063/1.1797541

Dobrowolski, J. A., Ho, F. C., & Waldorf, A. (1983). Determination of optical constants of thin film coating materials based on inverse synthesis. *Appl. Opt.*, *22*, 3191. http://dx.doi.org/10.1364/AO.22.003191

Dragoman, D., & Dragoman, M. (2002). *Optical Characterization of Solids*, Berlin: Springer-Verlag

Dressel, M., & Grüner, G. (2002). *Electrodynamics of Solids: Optical Properties of Electrons in Matter*. Cambridge: Cambridge University Press

Dresselhaus, M. S. (2001). *Solid State Physics: Part 2: Optical Properties of Solid*

El-Naggar, A. M., El-Zaiat, S. Y., & Hassan, S. M. (2009). Optical parameters of epitaxial GaN thin film on Si substrate from the reflection spectrum. *Optics and Laser Technol.*, *41*, 334. http://dx.doi.org/10.1016/j.optlastec.2008.05.022

El-Nahass, M. M., El-Sayed, H. E. A., & El-Barry, A. M. A. (2006). Transport mechanisms and photovoltaic characteristics of p-$S_xSe_{100-x/n}$-Si heterojunctions. *Solid State Electron.*, *50*(3), 355-361. http://dx.doi.org/10.1016/j.sse.2006.01.011

El-Zawawi, I. K., & Abd-Alla, R. A. (1999). Electrical and optical phototransformation properties in As-doped Se thin films. *Thin Solid Films*, *339*, 314-319. http://dx.doi.org/10.1016/S0040-6090(98)01324-8

Epstein, K. A., Misemer, D. K., & Vernstrom, G. D. (1987). Optical parameters of absorbing semiconductors from transmission and reflection. *Appl. Opt.*, *26*, 294-299. http://dx.doi.org/10.1364/AO.26.000294

Erarslan, N., & Gungor, T. (2010). The determination of the thickness and optical constants of the ZnO crystalline thin film by using pointwise unconstrained minimization algorithm. *J. Graduate School Natural Appl. Sci. Mehmet Akif Ersoy Univ.*, *1*(2), 181-193

Forouhi, A. R., & Bloomer, I. (1986). Optical dispersion relations for amorphous semiconductors and amorphous dielectrics. *Phys. Rev. B*, *34*, 7018. http://dx.doi.org/10.1103/PhysRevB.34.7018

Forouhi, A. R., & Bloomer, I. (1988). Optical properties of crystalline semiconductors and dielectrics. *Phys. Rev. B*, *38,* 1865. http://dx.doi.org/10.1103/PhysRevB.38.1865

González-Leal, J. M., Márquez, E., Bernal-Oliva, A. M., Ruiz-Pérez, J. J. & Jiménez-Garay, R. (1998). Derivation of the optical constants of thermally-evaporated uniform films of binary chalcogenide glasses using only their reflection spectra. *Thin Solid Films*, *317*, 223-227. http://dx.doi.org/10.1016/S0040-6090(97)00519-1

Grenet, J., Larmagnac, J. P., & Michon, P. (1980). Aging and crystallization of evaporated amorphous selenium films. *Thin Solid Films*, *67*(1), L17-L20. http://dx.doi.org/10.1016/0040-6090(80)90309-0

Heavens, O. S. (1991). *Optical Properties of Thin Solid Films.* New York: Dover Publications

Innami, T., & Adachi, S. (1999). Structural and optical properties of photocrystallized Se films. *Phys. Rev. B*, *60*, 8284-4289. http://dx.doi.org/10.1063/1.370898

Innami, T., Miyazaki, T., & Adachi, S. (1999). Optical constants of amorphous Se. *J. Appl. Phys.*, *86*, 1382. http://dx.doi.org/10.1063/1.370898

Ishida, K., & Tanaka, K. (1997). Photoinduced anisotropic crystallization of amorphous Se. *Phys. Rev. B*, *56*, 206-209. http://dx.doi.org/10.1103/PhysRevB.56.206

Ito, H., Oka, M., Ogino, T., Takeda, A., & Mizushima, Y. (1982). Selenium thin film solar cell. *Jap. J. Appl. Phys.*, *21*, 77-81. 3rd photovoltaic science and engineering Conf. Japan, Kyoto, Suppl. 21-2

Iyayi, S. E., & Oberafo, A. A. (2005). Studies on a-Se/n-Si and a-Te/n-Si heterojunctions. *J. Appl. Sci. Environ. Mgt.*, *9*(1), 143-145.

Jackson, J. D. (1998). *Classical Electrodynamics* (3nd edn). Wiley & Sons, Inc.

Jafar, M. M. A-G. (2013). Comprehensive formulation forth total normal-incidence optical reflectance and transmittance of thin films laid on thick substrates. *European Int. J. Sci. Technol.*, *2*, 274

Jellison, G. E., & Modine, F. A., (1996). Parameterization of the optical functions of amorphous materials in the interband region. *Appl. Phys. Lett.*, *69*, 371. http://dx.doi.org/10.1063/1.118064

Joo, H-Y., Kim, H. J., Kim, S. J., & Kim, S. Y. (1999). Spectrophotometric analysis of aluminum nitride thin films. *J. Vac. Sci. Technol. A*, *17*, 862-870. http://dx.doi.org/10.1116/1.582035

Joshi, S. S., & Lokhande, C. D. (2006). Fabrication of isotype (p-p) selenium–polyaniline heterojunction diode by electrochemical method. *Appl. Surf. Sci. 252*(24), 8539-8543. http://dx.doi.org/10.1016/j.apsusc.2005.11.070

Kasap, S. O. (2002). *Handbook of Imaging Materials* (2nd edn), revised and expanded ed., Diamond, A. S., & Weiss, D. S. New York: Marcel Dekker Inc., chapter 9

Kasap, S. O., & Juhasz, C. (1986). Kinematical transformations in amorphous selenium alloys used in xerography. *J. Mater. Sci.*, *21*(4), 1329-1340. http://dx.doi.org/10.1007/BF00553271

Kasap, S. O., & Rowlands, J. A. (2000). Review X-ray photoconductors and stabilized a-Se for direct conversion digital flat-panel X-ray image-detectors. *J. Mater. Sci.: Mater. Electron*., *11*(3), 179-198. http://dx.doi.org/10.1023/A:1008993813689

Kasap, S. O., Aiyah, V., & Yannacopoulos, S. (1990). Thermal and mechanical properties of amorphous selenium films in the glass transformation region. *J. Phys. D: Appl. Phys.*, *23*, 553-561. http://dx.doi.org/10.1088/0022-3727/23/5/013

Kasap, S. O., Rowlands, J. A., Tanioka, K., & Nathan, A. (2006). *Charge Transport in Disordered Solids with Applications in Electronics*. ed Baranovskii, S. Chichester: Wiley and Sons, chapter 4

Kasap, S., & Capper, P. (2006). *Optical properties of electronic materials: Fundamentals and characterization*. Springer handbook of electronic and photonic materials, Springer, Chapter 3

Klein, J. D., Yen, A., & Cogan, S. F. (1990). Determining thin film properties by fitting optical transmittance. *J. Appl. Phys.*, *68*, 1825. http://dx.doi.org/10.1063/1.346617

Kolobov, A. V. (1996). On the origin of p-type conductivity in amorphous chalcogenides. *J. Non-Crystal. Solids*, *198-200*, 728-731. http://dx.doi.org/10.1016/0022-3093(96)00119-6

Kotkata, M. F., & Abdel-Wahab, F. A. (1990). Effect of structural defects on optical properties of amorphous selenium films. *J. Mater. Sci.*, *25*(5), 2379-2388. http://dx.doi.org/10.1007/BF00638031

Kotkata, M. F., Abdel-Wahab, F. A., & Al-Kotb M. S. (2009). Effect of In-content on the optical properties of a-Se films. *Appl. Surface. Sci.*, *255*(22), 9071-9077. http://dx.doi.org/10.1007/BF00638031

Kubota, M., Kato, T., Suzuki, S., Maruyama, H., Shidara, K., Tanioka, K., Sameshima, K., Makishima, T., Tsuji, K., Hirai, T., & Yoshida, T. (1996). Ultrahigh-sensitivity New Super-HARP camera. *IEEE Trans. Broadcasting*, *42*(3), 251-258. http://dx.doi.org/10.1109/11.536588

Kukinyi, M., Benkö, N., Grofcsik, A., & Jones, W. J. (1996). Determination of the thickness and optical constants of thin films from transmission spectra. *Thin Solid Films*, *286*, 164-169. http://dx.doi.org/10.1016/S0040-6090(96)08737-8

Lakshmi, M. (2001). Studies on chemical bath deposited semiconducting copper selenide and iron sulfide thin films useful for photovoltaic applications. *PhD Thesis* Cochin University of Science and Technology, India

Larmagnac, J. P., Grenet, J., & Michon, P. (1981). Glass transition temperature dependence on heating rate and on ageing for amorphous selenium films. *J. Non-Crystal. Solids*, *45*(2), 157-168. http://dx.doi.org/10.1016/0022-3093(81)90184-8

Liang, W. Y., & Beal, A. R. (1976). A study of the optical joint density-of-state function. *J. Phys. C: Solid State Phys.*, *9*, 2823. http://dx.doi.org/10.1088/0022-3719/9/14/020

Manifacier, J. C., Gasiot, J., & Fillard, J. P. (1976). A simple method for the determination of the optical constants n, k and the thickness of a weakly absorbing thin film. *J. Phys. E: Sci. Instrum.*, *9*, 1002. http://dx.doi.org/10.1088/0022-3735/9/11/032

Márquez, E., Bernal-Oliva, A. M., González-Leal, J. M., Prieto-Alcón, R., Ledesma, A., Jiménez-Garay, R., & Mártil. I. (1999). Optical-Constant Calculation of Non-Uniform Thickness Thin Films of the $Ge_{10}As_{15}Se_{75}$ Chalcogenide glassy alloy in the Sub-Band-Gap Region (0.1 – 1.8 eV). *Mater. Chem. Phys.*, *60*, 231-239. http://dx.doi.org/10.1016/S0254-0584(99)00078-4

Márquez, E., Ramirez-Malo, J. B., Villares, P., Jiménez-Garay, R. & Swanepoel, R. (1995). Optical Characterization of Wedge-Shaped Thin Films of Amorphous Arsenic Trisulphide Based only on their Shrunk Transmission spectra. *Thin Solid Films*, *254*, 83-91. http://dx.doi.org/10.1016/0040-6090(94)06267-O

Minkov, D. A. (1990). Computation of the Optical Constants of a Thin Dielectric Layer from the Envelopes of the Transmission Spectrum, at Inclined Incidence of the Radiation. *J. Modern Optics*, *37*, 1977. http://dx.doi.org/10.1080/09500349014552181

Mott, N. F. & Davis, E. A. (1979). *Electronic Processes in Non-Crystalline Materials* (2nd edn). Oxford: Clarendon Press

Mukolu, A. I. (2004). Oxygen–induced barrier height changes in aluminum–amorphous selenium Schottky diodes. *Botswana, J. Technol.*, *13*(1), 51-54. http://dx.doi.org/10.4314/bjt.v13i1.15384

Mulama A. A., Mwabora J. M., Oduor A. O., & Muiva C. C. (2014). Optical properties and Raman Studies of Amorphous Se-Bi Thin Films. *The African Review Phys*., *9*, 33-38

Mulato, M., Chambouleyron, I., Birgin, E. G., & Martínez, J. M. (2000). Determination of thickness and optical constants of amorphous silicon films from transmittance data. *Appl. Phys. Lett.*, *77*, 2133-2135. http://dx.doi.org/10.1063/1.1314299

Nagels, P., Sleeckx, E., Callaerts, R., & Tichy, L. (1995). Structural and optical properties of amorphous selenium prepared by plasma-enhanced CVD. *Solid State Commun.*, *94*, 49-52. http://dx.doi.org/10.1016/0038-1098(95)00014-3

Nagels, P., Sleeckx, E., Callaerts, R., Marquez, E., Gonzalez, J. M., & Bernal-Oliva, A. M. (1997). Optical Properties of Amorphous Se Films Prepared by PECVD. *Solid State Commun.*, *102*, 539-543. http://dx.doi.org/10.1016/S0038-1098(97) 00053-7

Navarrete, G., Marquez, H., Cota, L., Siqueiros, J., & Machorro, R. (1990). Determination of the optical properties of amorphous selenium films by a classical damped oscillator model. *Appl. Opt.*, *29*, 2850-2852. http://dx.doi.org/10.1364/AO.29.002850

Nichelatti, E. (2002). Complex refractive index of a slab from reflectance and transmittance: analytical solution. *Journal of Optics A: Pure and Applied Optics. 4*, 400-403. http://dx.doi.org/10.1088/1464-4258/4/4/306

O'Leary, S. K., Johnson, S. R., & Lim, P.K. (1997). The relationship between the distribution of electronic states and the optical absorption spectrum of an amorphous semiconductor: An empirical analysis. *J. Appl. Phys.*, *82* (7), 3334-3340. http://dx.doi.org/10.1063/1.365643

Palik, E. D. (1998). *Handbook Optical Constants of Solids*. San Diego: Academic Press

Pejova, B., & Grozdanov, I. (2001). Solution growth and characterization of amorphous selenium thin films: Heat transformation to nanocrystalline gray selenium thin films. *Appl. Surf. Sci.*, *177*, 152-157. http://dx.doi.org/10.1016/S0169-4332(01)00191-X

Peng, C. H., & Desu, S. B. (1994). Modified method for obtaining optical properties of weakly absorbing thin films and its application to thin films Pb (Zr, Ti) O3 solid solutions. *J. Am. Ceram. Soc.*, *77*, 929-938. http://dx.doi.org/10.1111/j.1151-2916.1994.tb07249.x

Poborchii, V. V., Kolobov, A. V., & Tanaka, K. (1998). An in situ Raman study of polarization-dependent photocrystallization in amorphous selenium films. *Appl. Phys. Lett*., *72*, 1167. http://dx.doi.org/10.1063/1.121002

Poelman, D., & Smet, P. F. (2003). Methods for the determination of the optical constants of thin films from single transmission measurements: a critical review. *J. Phys. D: Appl. Phys.*, *36*, 1850. http://dx.doi.org/10.1088/0022-3727/36/15/316

Pradeep, J. A., & Agarwal, P. (2010). Determination of thickness, refractive index, and spectral scattering of an inhomogeneous thin film with rough interfaces. *J. Appl. Phys.*, *108*, 043515. http://dx.doi.org/10.1063/1.3478706

Press, W. H., Teukolsky, S. A., Vettering, W. T., & Flannery, P. B. (1992). *Numerical recipes in C*, Cambridge University Press, New York

Reitz, J. R., Milford, F. J., & Christy, R. W. (1993). *Foundation of Electromagnetic Theory* (4th edn). Addison-Wesley Publishing Company, Inc.

Richards, B. S. (1998). *Optical Characterization of Sputtered Silicon Thin Films for Photovoltaic Application*. *MSc. Thesis*. University of New South Wales, Australia

Richards, B. S., Lambert, A., & Sproul, A. B. (2004). Determination of the optical properties of non-uniformly thick non-hydrogenated sputtered silicon thin films on glass. *Thin Solid Films*, *460*, 247-255. http://dx.doi.org/10.1016/j.tsf.2004.01.072

Rogalski, M. S., & Palmer, S. B. (2000). *Solid State Physics*. Gordon and Breach Science Publishers

Ruíz-Pérez, J. J., González-Leal, J. M., Minkov, D. A., & Márquez, E. (2001). Method for determining the optical constants of thin dielectric films with variable thickness using only their shrunk reflection spectra. *J. Phys. D: Appl. Phys.*, *34*, 2489. http://dx.doi.org/10.1016/j.tsf.2004.01.072

Solieman, A. S., Hafiz M. M., Abu-Sehly, A. A., & Alfaqeer A. A. (2014). Dependence of optical properties on the thickness of amorphous $Ge_{30}Se_{70}$ thin films. *Journal of Taibah University for Science*, *8*(3), 282-288. http://dx.doi.org/10.1016/j.jtusci.2014.01.002

Solieman, A., & Abu-Sehly, A. A. (2010). Modelling of optical properties of amorphous selenium thin films. *Physica B, 405*, 1101-1107. http://dx.doi.org/10.1016/j.physb.2009.11.014

Sólyom, J. (2009). *Fundamentals of the Physics of Solids. Volume 2- Electronic Properties*. Springer-Verlag, Berlin

Stenzel, O. (2005). *The Physics of Thin Film Optical Spectra: An Introduction*. Berlin: Springer-Verlag

Swanepoel, R. (1983). Determination of the thickness and optical constants of amorphous silicon. *J. Phys. E: Sci. Instrum.*, *16*, 1214. http://dx.doi.org/10.1088/0022-3735/16/12/023

Swanepoel, R. (1984). Determination of surface roughness and optical constants of inhomogeneous amorphous silicon films. *J. Phys. E: Sci. Instrum.*, *17*, 896. http://dx.doi.org/10.1088/0022-3735/17/10/023

Tan, W. C. (2006). Optical properties of amorphous selenium films. University of Saskatchewan, Saskatoon, Canada.

Tan, W. C., Belev, G., Koughia, K., Johanson, R., O'Leary, S. K., & Kasap, S. (2007). Optical Properties Vacuum Deposited and Chlorine Doped a-Se Thin Films: Aging Effect. *J. Mater. Sci.: Mater. Electron.*, *18*, 429-433. http://dx.doi.org/10.1007/s10854-007-9227-3

Tan, W. C., Koughia, K., Singh, J. & Kasap, S. O. (2006) *Optical Properties of Condensed Matter and Applications*. ed Singh, J. London: John Wiley, chapter 1

Tauc, J. (1972) *Optical Properties of Solids*, ed. Abelés, F. Amsterdam: North-Holland

Tauc, J. (1979) *Amorphous and Liquid Semiconductors.* New York: Plenum Press

Theiss, W., Hard- and Software (Manual 2012), (http://www.mtheiss.com)

Tichy, L., Ticha, H., Nagels, P., Sleeckx, E., & Callaerts, R. (1996). Optical gap and Urbach edge slope in a-Se. *Mater. Lett.*, *26*, 279-283. http://dx.doi.org/10.1016/0167-577X(95)00234-0

Tigau, N. (2006). Substrate temperature effect on the optical properties of amorphous Sb_2S_3 thin films. *Crys. Res. Technol.*, *41,* 474. http://dx.doi.org/10.1002/crat.200510608

Tonchev, D., & Kasap, S. O. (2002). Effect of aging on glass transformation measurements by temperature modulated DSC. *Materials Science and Engineering A*, *328*, 62-66. http://dx.doi.org/10.1016/S0921-5093(01)01668-9

Touihri, S., Safoula, G., & Bernede, J. C. (1997). Diode Devices Based on Amorphous Selenium Films. *Phys. Status Solidi* (a), *159*(2), 569-578. http://dx.doi.org/10.1002/1521396x(199702)159:<569::AID-PSSA569>3.0.CO;2-x

Truong, V. V., & Tanemura, S. (2006). *Optical Properties of Condensed Matter and Applications* ed. Singh, J. Chichester: John Wiley, chapter 13

Vautier, C., Slater, J. M., & Derrey, T. (1988). Nature of defects in amorphous Bi-Se alloys. *J. Non-Crystal. Solids*, *103*(1), 65-72. http://dx.doi.org/10.1016/0022-3093(88)90416-4

Ventura, S. D., Birgin, E. G., Martinez, J. M., & Chambouleyron, I. (2005). Optimization techniques for the estimation of the thickness and the optical parameters of thin films using reflectance data. *J. Appl. Phys.*, *97*, 043512. http://dx.doi.org/10.1063/1.1849431

Wang, K., Chen, F., Belev, G., Kasap, S., & Karim, K. S. (2009). Lateral metal-semiconductor-metal photodetectors based on amorphous selenium. *Appl. Phys. Lett.*, *95*, 013505. http://dx.doi.org/10.1063/1.3173818

Wang, K., Chen, F., Belev, G., Kasap, S., & Karim, K. S. (2009). Design and modeling of a lateral a-Se MSM photoconductor as indirect conversion X-ray imager. *Proc. SPIE*, *7449*, 74491W. http://dx.doi.org/10.1117/12.829299

Wang, K., Chen, F., Shin, K-W., Allec, N., & Karim, K. S. (2010). Lateral amorphous selenium metal-semiconductor-metal photodetector for large-area high-speed indirect-conversion medical imaging applications. *Proc. SPIE*, *7622*, 762217. http://dx.doi.org/10.1117/12.843980

Ward, L. (1994). *The Optical Constants of Bulk Materials and Films* (2nd edn). Bristol: Institute of Physics Publishing

Wemple, S. H., & DiDomenico, M. (1971). Behavior of the electronic dielectric constant in covalent and ionic materials. *Phys. Rev. B*, *3*, 1338. http://dx.doi.org/10.1103/PhysRevB.3.1338

Zhao, W., Hunt, D. C., Kenkichi, T., & Rowlands, J. A. (2005). Amorphous selenium flat panel detectors for medical applications. *Nucl. Instrum. Meth. Phys. Res. A*, *549*(1-3), 205-209. http://dx.doi.org/10.1016/j.nima.2005.04.053